Forest Ecology and Management 557 (2024) 121765

Contents lists available at ScienceDirect

Forest Ecology and Management

journal homepage: www.elsevier.com/locate/foreco

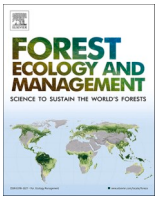

Integration of tree-ring data, Landsat time series, and ALS-derived topographic variables to quantify growth declines in black spruce

Alexandre Morin-Bernard [a,*], Alexis Achim [a], Nicholas C. Coops [b], Joanne C. White [c]

[a] Department of Wood and Forest Sciences, Université Laval, 2425 rue de la Terrasse, Québec, QC G1V 0A6, Canada
[b] Department of Forest Resources Management, University of British Columbia, 2424 Main Mall, Vancouver, BC V64T 1Z4, Canada
[c] Canadian Forest Service (Pacific Forestry Centre), Natural Resources Canada, 506 West Burnside Road, Victoria, BC V8Z 1M5, Canada

ARTICLE INFO

Keywords:
Landsat
Airborne laser scanning
Tree rings
Drought
Eastern spruce budworm

ABSTRACT

Forest ecosystems and timber products are expected to play a determining role in climate change mitigation and adaptation. As the frequency and severity of natural disturbances increase, remote sensing technologies prove crucial for detecting and assessing the impact of natural disturbance on forest condition and productivity. Although satellite-based remote sensing is commonly used for measuring the extent and severity of stand-replacing disturbances such as fire and harvest, capturing the effects of subtler, non-stand replacing disturbances (NSR) remains challenging. Studies based on the analysis of tree rings have yielded insights on the impact of such disturbances at a local scale, yet tools for estimating the compound impact of NSR disturbances on broader scales are lacking. The objective of this study was to use Landsat time series spectral reflectance information in conjunction with tree-ring data to generate spatially explicit estimates of growth declines attributable to NSR disturbances at a 30-meter resolution across black spruce-dominated stands in two managed boreal forests. Basal area increment (BAI) calculated from 1545 increment cores collected in 52 plots across the two study sites were used to assess the growth decline in each plot due to NSR disturbance events from drought and insect defoliation. Plots that experienced a severe growth decline were identified using a threshold (i.e., a decrease in BAI $\geq$ 23.7% between two consecutive 11-year periods) established after examining the historical variability in growth rates from the tree-ring data. Subsequently, a logistic regression model was developed to predict the probability of a plot sustaining a severe growth decline, using predictors from Landsat time series and topographic variables derived from airborne laser scanning data, achieving an accuracy of 79.2% after five-fold cross-validation. In a subsequent modelling step, plots that experienced severe declines in BAI were used to construct a linear model, predicting the magnitude of the decline in BAI attributed to NSR disturbances using predictors from Landsat time series, and resulting in a model with an $R^2 = 0.70$ when using five-fold cross-validation. Model predictions were then applied to black spruce-dominated stands at both study sites to estimate the impact of disturbances on forest productivity. Depending on the study site, between 22.6% and 57.6% of the analysis area had a predicted probability of severe growth decline > 50%. Within the most affected areas, the median decrease in annual BAI predicted using the OLS model was 95.3 and 64.4 $mm^2\ yr^{-1}$, respectively, for the two study sites. This research demonstrates the utility of combining tree ring and Landsat data to assess the impact of non-stand-replacing disturbances on forest growth at the scale of a forest management unit that in turn could inform salvage and/or silvicultural interventions that enhance the resistance and resilience of vulnerable stands.

1. Introduction

Forest ecosystems and timber products are expected to play a determining role in climate change mitigation strategies (Nabuurs et al., 2007; Smyth et al., 2014). Boreal forests represent approximately one-third of the world's forested area, and similar proportions of the global terrestrial biogenic carbon stock and lumber produced worldwide (Brandt et al., 2013; Gauthier et al., 2015; Pan et al., 2011). The successional pathways, species composition, and carbon balance of boreal forested ecosystems are driven by natural and anthropogenic

* Corresponding author.
E-mail address: alexandre.morin-bernard@sbf.ulaval.ca (A. Morin-Bernard).

https://doi.org/10.1016/j.foreco.2024.121765
Received 8 December 2023; Received in revised form 5 February 2024; Accepted 7 February 2024
Available online 15 February 2024

disturbances from fires, harvests, wind events, insect outbreaks, and drought (Aakala et al., 2023; Wang et al., 2021; White et al., 2017). The increasing severity, extent, and frequency of these disturbances, along with changes in forest productivity due to rising temperatures, increasing CO_2, and shifts in water dynamics, present a significant threat to the ability of boreal forests to effectively mitigate climate change and sustain timber supply (Brecka et al., 2018; McDowell et al., 2020; Seidl et al., 2017).

The contiguous boreal forests of Canada account for almost 30% of the country's land area (Brandt et al., 2013). Black spruce (*Picea mariana* (Mill) B.S.P.) is the predominant tree species contributing to over 35% of the merchantable wood volume harvested in the provinces of Quebec and Ontario alone (MFFP, 2018b; MNRF, 2021). Although stand-replacing disturbances such as fire and harvest are major drivers of the succession and renewal of these black spruce stands, the influence of lower severity, non-stand replacing (NSR) disturbances is also substantial (Aakala et al., 2023; Harper et al., 2002). In particular, changes in water availability and rising temperatures have detrimental impacts on the growth and survival of black spruce stands, especially in the warmer regions of the boreal biome (Berner and Goetz, 2022; Chagnon et al., 2022; D'Orangeville et al., 2018; Marchand et al., 2019), which are experiencing more frequent water deficits that can lead to increased mortality rates (Peng et al., 2011; Sánchez-Pinillos et al., 2022). These black spruce forests are also experiencing eastern spruce budworm outbreaks (*Choristoneura fumiferana* Clem.), a defoliating insect primarily targeting balsam fir (*Abies balsamea* (L.) Mill), that also significantly impacts the growth of black spruce at epidemic levels (Blais, 1957; Hennigar et al., 2008; Régnière et al., 2012; Sánchez-Pinillos et al., 2019) with damage often varying topographically. Higher elevations, for instance, are generally associated with a lower probability of defoliation by the spruce budworm, especially during the onset of the outbreaks (Bouchard and Auger, 2014; Magnussen et al., 2004). The interaction effects of defoliation and lack of water on the growth of black spruce stands is complex and remains largely unquantified (Canelles et al., 2021; Itter et al., 2019; Lacey and Dech, 2012), however it is recognised that drought conditions preceding spruce budworm outbreaks increase the overall severity of the impact (Bouchard et al., 2018; De Grandpré et al., 2019; Jactel et al., 2012). Quantifying alterations in black spruce growth caused by the compound effects of drought and defoliation is therefore important to provide a more comprehensive picture of how these forests will respond to future climate.

Remote sensing technologies provide wall-to-wall information on forest condition, allowing for a near-real time monitoring of disturbances over large geographical extents (Senf et al., 2017; Woodcock et al., 2020). With its open-access policy, high radiometric and geometric qualities and moderate spatial resolution, imagery from the Landsat program of satellites is now widely used to detect and characterise changes in forest condition (Banskota et al., 2014; Woodcock et al., 2008; Wulder et al., 2022). The impact of NSR disturbances such as insect defoliation and drought is typically more subtle to detect from these time series of spectral data when compared to stand-replacing disturbances such as fires or harvesting, as it typically does not result in a complete loss of the forest cover (Ahmed et al., 2017; Hermosilla et al., 2015b; White et al., 2017). Depending on the severity of the disturbance, stands can experience thinning and discoloration of the foliage, as well as alterations of stand structural attributes because of increased snags, broken treetops and dropped branches (Coops et al., 2020).

Approaches to detect NSR disturbances from satellite spectral data include direct comparisons of canopy reflectance properties before and after the event (e.g. Franklin et al., 2001; Olthof et al., 2004), as well as more refined spectral trajectory-based methods, which analyse the trajectory of spectral values over time and identify the start and severity of a disturbance event from a deviation from expected spectral values (e.g. Hermosilla et al., 2015a; Kennedy et al., 2010; Mulverhill et al., 2023; Zhu and Woodcock, 2014). These later methods have successfully been applied in Canada and globally to map the severity of damage from defoliator insects and bark beetles (e.g. Coops et al., 2020; Dottavio and Williams, 1983; Rodman et al., 2021; Senf et al., 2015), and to characterise the impact of drought events and changes in water availability on forest condition (e.g. Bell et al., 2018; Berner and Goetz, 2022; Vogelmann et al., 2016). While these studies have generated spatially explicit information on the timing, severity, persistence, and extent of NSR disturbances, less emphasis has been placed on assessing the impact on forest growth.

Dendrochronology, the science of dating and studying past events and environmental changes through the analysis of tree rings (Guibal and Guiot, 2021), allows an accurate reconstruction of past tree growth at an annual or even sub-annual scale and in turn precise assessments of the impact of NSR disturbances such as drought and insect defoliation from field based, rather than satellite observations (Altman, 2020; Biondi, 1999; Nehrbass-Ahles et al., 2014). Dendrochronological methods have been used to reconstruct the history of eastern spruce budworm outbreaks (e.g., Boulanger and Arseneault, 2004; Itter et al., 2019; Lacey and Dech, 2012) and drought events (e.g., Aakala et al., 2023; Archambault and Bergeron, 1992; Girardin et al., 2008) in boreal forests as well as to quantify the losses in carbon stocks attributable to NSR disturbances (Klesse et al., 2016). Recent advances have seen the development of specific tree-ring data collection and analysis protocols that allow for reliable stand-level reconstructions of past growth trends (Babst et al., 2018; Klesse et al., 2016; Nehrbass-Ahles et al., 2014).

Several studies have built links between tree-ring chronologies and satellite spectral trajectories (Babst et al., 2010; Bonney and He, 2021; Decuyper et al., 2020; Lopatin et al., 2006; Vicente-Serrano et al., 2016) with promising results observed when assessing trends in, for example, growth and forest primary productivity (Babst et al., 2018; Nehrbass-Ahles et al., 2014). Although the existence of relationships between forest growth and satellite data has been confirmed, the potential to employ Landsat time series for quantifying changes in growth rates attributable to NSR disturbances remains relatively unexplored. Yet, such information is critical to forest management decision-making, since severe growth declines may be early warning signals of mortality (Anderegg et al., 2019; Kéfi et al., 2013; Mamet et al., 2015). Accurate and spatially explicit information regarding the impact of NSR disturbances on forest growth could be employed, for instance, to plan salvage operations to harvest dying trees, or to implement targeted silvicultural interventions to enhance the resistance and resilience of vulnerable stands (Achim et al., 2022; Moreau et al., 2022; Wotherspoon et al., 2022b).

Our objective was to exploit Landsat time series reflectance information in combination with tree-ring observations to produce spatially explicit estimates of growth declines due to NSR disturbances at a 30 m resolution across black spruce dominated stands in two managed boreal forests in Canada. In addition, we aimed to identify the most significant Landsat-derived vegetations indices and examined if the inclusion of topographic information derived from airborne laser scanning (ALS) data improved the performance of the approach compared to models based exclusively on satellite data. To limit the effect of variations in response to NSR disturbances among species, as well as to limit the effect of stand development stages on growth rates, we focused on fire-origin, black spruce dominated (i.e., $>$ 75% of the basal area) stands, currently at the end of the stem exclusion stage or at the early understory onset of the reinitiation stage. Trees in these stands grew as a single cohort following severe wildfires that decimated the previous stand. Depending on site productivity, the transition from the stem exclusion to the understory reinitiation stages in black spruce stands occurs between approximately 50–120 years after stand establishment (Harper et al., 2005; Lieffers et al., 2003). Targeting stands at this stage of development enabled us to avoid those stands where the presence of canopy gaps caused by the mortality of dominant trees, which would lead to the growth of a second cohort of trees and the development of an uneven-aged structure (Harper et al., 2005; Oliver and Larson, 1996).

The complex competition dynamics within uneven-aged stands might have increased the variability of responses to disturbances among trees due to age, and could have increased the bias due to sampling only the surviving trees (Nehrbass-Ahles et al., 2014; Primicia et al. 2015; Šamonil et al. 2015).

2. Material and methods

2.1. Study sites

The study was conducted in two forest management areas in the Canadian boreal forest. The first study site, Lac Saint-Jean (LSJ), is located north of Lac Saint-Jean in the province of Quebec (Fig. 1). The site covers 867,107 ha encompassing two bioclimatic domains: the balsam fir-paper birch domain to the south, and the spruce-feathermoss domain to the north (Saucier et al., 2010). Based on historical means for the 1981–2010 period, the average annual temperature is 0.8°C and the region receives an annual average precipitation of 928 mm (Wotherspoon et al., 2022a). Climate projections made using an ensemble of thirteen global circulation models and averaged under four shared socioeconomic pathway (i.e. SSPs 1–4) scenarios (Mahony et al., 2022) indicate that maximum daily temperatures are expected to increase by 3.0–4.2°C in this region by 2050, while summer maximum temperature could increase by 2.1–2.9°C. Annual precipitation is projected to increase by an average of 18% in the same period, but the increase will be considerably smaller in the southern portion of the study site (Wotherspoon et al., 2022a). Forest management activities include both partial harvest and clearcutting, as well as pre-commercial thinning and restocking when natural regeneration is not sufficient. The dominant tree species are black spruce, balsam fir, jack pine (*Pinus banksiana* Lamb), tamarack (*Larix laricina* (Du Roi) K. Koch), paper birch (*Betula papyrifera* Marshall) and trembling aspen (*Populus tremuloides* Michx.).

The second study site is the Romeo Malette Forest management unit (RMF), in the province of Ontario (Fig. 1). It covers 586,607 ha within the Lake Abitibi ecoregion in the Ontario Shield ecozone (Wester et al., 2018). The dominant tree species include black spruce, jack pine, white spruce (*Picea glauca* (Moench) Voss), aspen, and paper birch. The forest also has components of balsam fir, cedar (*Thuja occidentalis* L.), tamarack, and white and red pines (*Pinus strobus* L. and *Pinus resinosa* Soi ex. Aiton). Based on the historical mean for the 1981–2010 period, the mean annual temperature in the RMF site is 1.8°C and it receives 773 mm of precipitation annually, on average (Wotherspoon et al., 2022a). According to projections made using an ensemble of thirteen global circulation models averaged under four shared socioeconomic pathways (i.e. SSPs 1–4) scenarios (Mahony et al., 2022), both the minimum and maximum temperatures are expected to increase by 2.9°C on average in this region by 2050. The risk of drought and vulnerability to forest pests could increase due to warmer summers with no change in precipitation and warmer winters with reduced snowfall (Wotherspoon et al., 2022a).

2.1.1. Status of non-stand replacing disturbances at the study sites

Biotic disturbances in conifer-dominated stands at both study sites are mainly attributable to the eastern spruce budworm (Urquizo et al.,

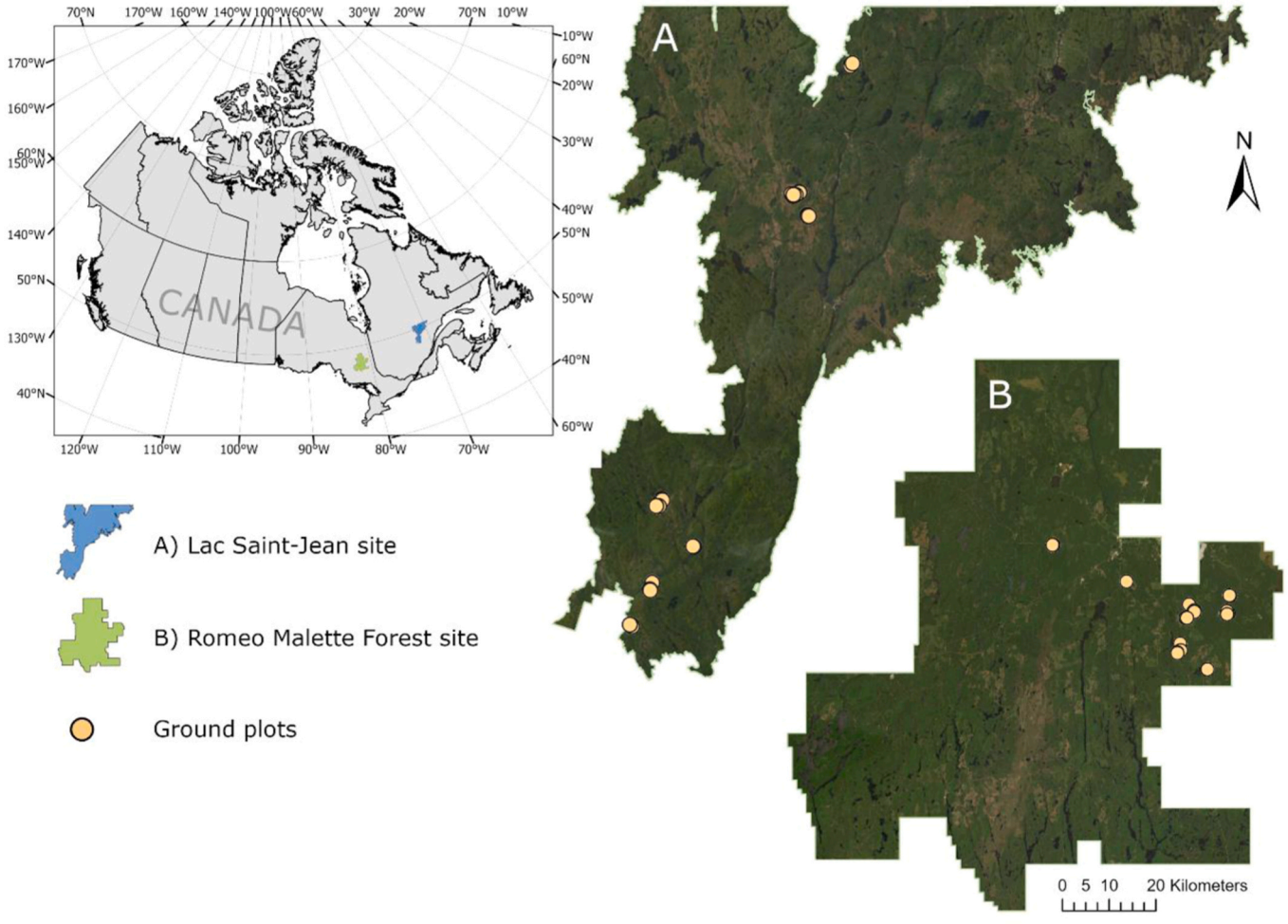

Fig. 1. Location of the Lac Saint-Jean (A, 28 plots) and the Romeo Malette Forest (B, 24 plots) study sites and the corresponding ground plot locations.

2000). Although the insect is endemic, outbreaks typically follow a cyclical pattern with a recurrence of 30–40 years (Boulanger and Arseneault, 2004; Régnière et al., 2012). Other insects, such as the Swaine jack pine sawfly (*Neodiprion swainei* Midd.), the yellowheaded spruce sawfly (*Pikonema alaskensis* (Rohwer)), and the forest tent caterpillar (*Malacosoma disstria* Hübner) have also caused significant damage in the past (MNRF, 2023b, MFFP, 2018). Wildfires are also major drivers of forest dynamics and succession with 27,500 ha burnt in 2005 alone, and 176,434 burned from 2005 to 2014 at the LSJ site. The most severe fire event recorded within the RMF site occurred in 2012, when around 40,000 ha were burned (MNRF, 2023a).

Data on the status of NSR disturbances within the two study sites was gathered from the available disturbance layers produced by the Ministère des Ressources Naturelles et des Forêts of Quebec (MRNF) and the Ontario Ministry of Natural Resources and Forestry (MNRF), as well as daily climate data extracted over the location of the ground plots to characterise drought conditions. Both sites were under an active spruce budworm outbreak at the time of sampling in 2021 (Fig. 2), as determined from aerial surveys. Such surveys are conducted on an annual basis by the MRNF and MNRF, providing georeferenced layers publicly available online (MNRF, 2023b; MRNF, 2023). At the LSJ site, initial detection of defoliation from spruce budworm occurred in 2006 but damage was minor until the 2011–2016 period when defoliated areas increased sharply, culminating in 2020 with a total of 575,476 ha affected within the study site, before decreasing slightly in the two following years (Fig. 2A; MRNF, 2023). The current budworm outbreak in the RMF site started in 2015 with areas of defoliation increasing sharply and continuously from 2019, with 180,184 ha affected as of 2021 (Fig. 2B; MNRF, 2023b).

To investigate how the occurrence of drought conditions evolved in the last decades, we examined values of the standardised precipitation evapotranspiration index (SPEI; Vicente-Serrano et al., 2010), a multi-scalar index based on temperature, and precipitation, which also consider the estimated cumulative water balance (Fig. 3). This index is frequently used in conjunction with tree-ring data to investigate the influence of drought on forest growth (DeSoto et al., 2020; Gazol et al., 2018; Wotherspoon et al., 2022b). Daily climate records from 1950 to 2021 at the location of each plot were imputed from the data of the six most representative surrounding weather stations using BioSim (Version 11; Régnière et al., 2017). We calculated SPEI values for the entire growing season according to the definition of McKenney et al., (2006), which is from May to October, for both of our study sites when using average daily temperature. Site-level SPEI time series were built by averaging the monthly index values calculated at the location of the ground plots established in each study site. This analysis revealed that the driest years over the period 1950–2021, defined as growing seasons during which the SPEI values were below the 5th percentile of historical values for this period, occurred in 1953, 2005, 2007, and 2010 at the LSJ site (Fig. 3A), and in 1955, 1997, 2005, and 2011 at the RMF site (Fig. 3B).

2.2. Plot establishment and data collection

We used data from the Quebec and Ontario provincial forest resource inventories (FRI; Bilyk et al., 2021; MRNF, 2022), high-resolution aerial images, and forest attribute layers derived from ALS data acquisitions conducted over the two study sites to identify potential forest stands for the field sampling. At the LSJ site, ALS data were acquired from 2018 to 2020 (during the growing season, leaf-on), using a full-waveform airborne laser scanner at an average density of 2.5 pts/m^2. The area-based approach, wherein ALS data and co-located field plots are used to predict a suite of forest inventory attributes (Næsset, 2002; White et al., 2013a), was applied at the LSJ site (Riopel et al., 2022). At the RMF site, ALS data were acquired in the summer of 2018, using a single photon laser scanner, with an average point density of 40.8 pts/m^2. The area-based approach was also applied at the RMF to predict a suite of forest inventory attributes (Queinnec et al., 2022). We used the provincial forest inventories and ALS-derived forest attributes to select mid-seral, black spruce dominated stands (≥75% BA) that originated from a fire and in which no harvest treatments have been carried out.

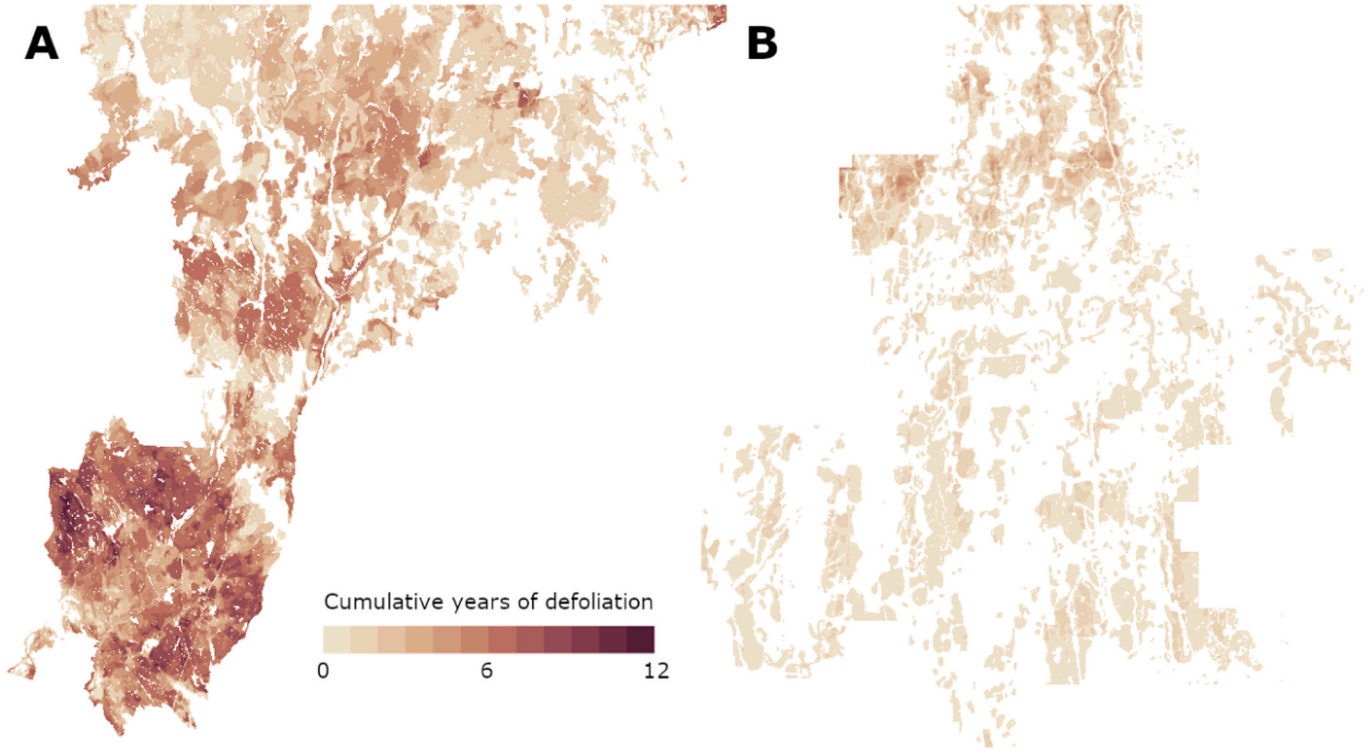

Fig. 2. Cumulative years of defoliation as of 2021 in the LSJ (A) and RMF (B) sites during the most recent eastern spruce budworm outbreak (MNRF, 2023a; MRNF, 2023).

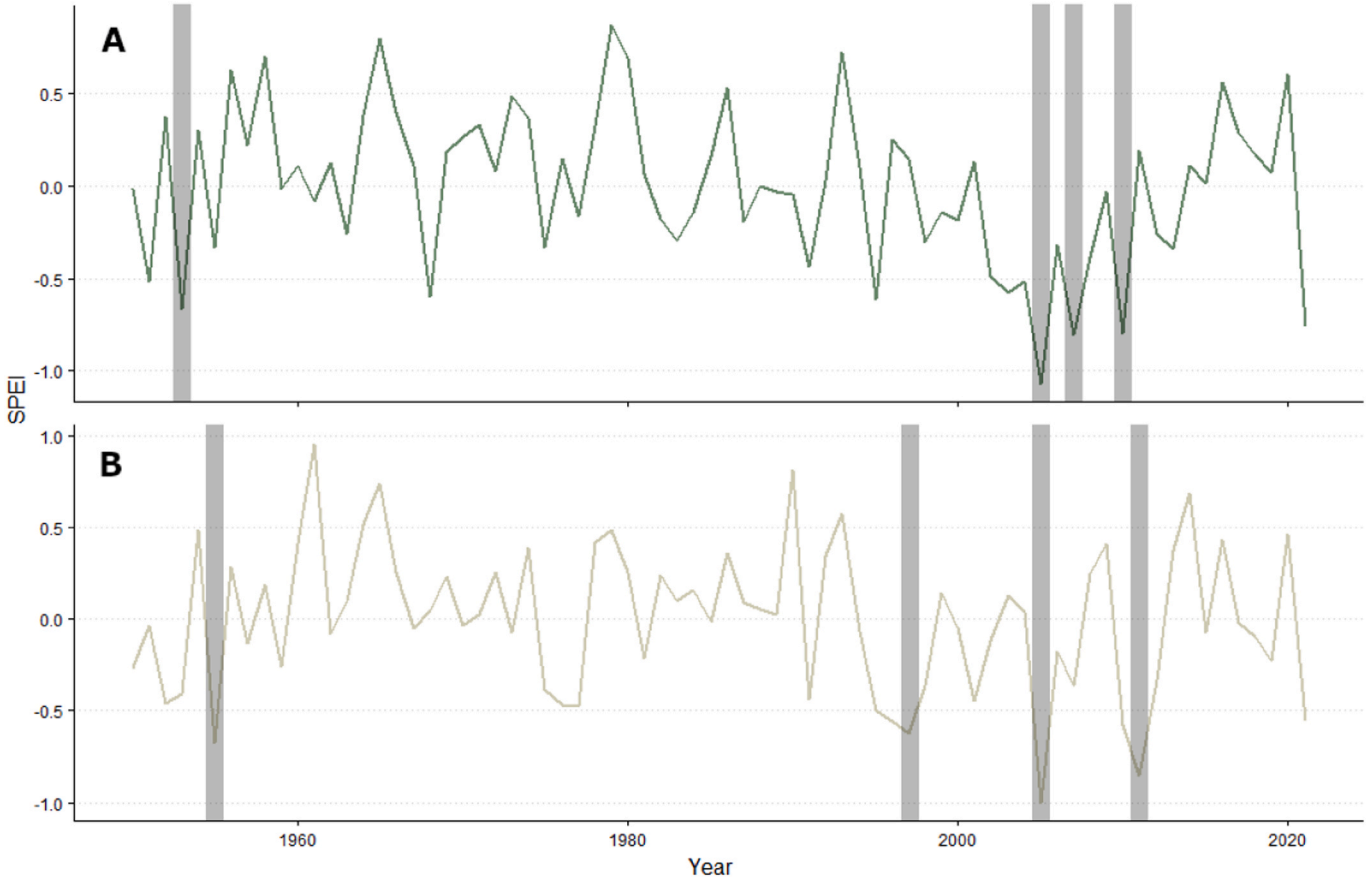

Fig. 3. Time series of the standardised precipitation evapotranspiration index (SPEI) at the LSJ (A) and RMF (B) sites. Shaded areas represent the driest years, defined as growing seasons during which the value of the SPEI was below the 5th percentile of historical values from 1950 to 2021.

Stands were then filtered using a minimum (80 m) and maximum (800 m) distance threshold from the main roads. All candidate plots (50 plots in LSJ site, 60 plots in RMF site) were then visited in the field, to confirm the even-aged structure and the wildfire origin of the stands, using the presence of a charcoal layer under the organic layer of the soil (Ohlson et al., 2009). This resulted in the exclusion of 22 plots in the LSJ site and 36 in the RMF site, either because the fire origin could not be confirmed, or because of the uneven age structure of the stands. A total of 52 plots (28 in the LSJ site and 24 in the RMF site) were measured during the summer of 2021 (Fig. 4).

We established 11.28 m radius (400 m^2) circular plots in which, for all living trees, the species and DBH were recorded. In addition to measurements of individual trees, the thickness of the humus layer and the coverage of herbaceous plants and mosses were measured. The location of each plot centre was recorded using a Trimble Geo7X precision GNSS connected to an external antenna, providing an estimated accuracy within 1 m for plot centre position after differential correction.

In each plot, 32 black spruce trees were randomly selected to be cored, as this approach best captures the population growth signal than sampling focussed on dominant/co-dominant trees (Babst et al., 2018; Biondi, 1999; Klesse et al., 2016; Nehrbass-Ahles et al., 2014). For each tree, the crown position and live crown ratio were recorded, and increment cores were collected at 1 m above the ground on the south side on 26 of the selected trees, while the remaining six trees were felled. A disc was collected on felled trees at a height of 1 m along the stem, which was added to the increment core samples for the measurement of past growth. A second disc was collected at the base of the stem to estimate the age of the stand.

2.3. Dendrochronological analysis

Increment cores were air-dried, and glued to wooden blocks, before being sanded, while discs were air dried and sanded. Ring widths were measured using a Velmex micrometer (± 0.002 mm) on all increment cores and discs. The dating accuracy was verified using the COFECHA program (Holmes, 1983). Time series of ring widths that did not cross-date with most other series in a plot were eliminated, resulting in between 24 and 32 usable ring series per plot measured from 1538 cores. Rejected samples were essentially cores damaged during the transport or that were presenting very narrow rings due to defoliation, creating uncertainty regarding the quality of the measurements.

The direct use of ring width measurements does not accurately reflect growth trends as it does not account for changes in trunk diameter over the lifespan of a tree (Biondi and Qeadan, 2008; Sullivan et al., 2016). To address this limitation, ring width measurements were converted into basal area increments (BAI), in mm^2yr^{-1}, which better reflects the evolution of growth rates and biomass accumulation over time (Babst et al., 2014; Biondi and Qeadan, 2008; Sullivan et al., 2016). Converting ring widths to BAI does not remove developmental effects on growth, but was appropriate for the current study conducted on even-aged stands, considering that BAI remains relatively stable during the mature phase of growth (Chen et al., 2002; Harper et al., 2005). A decline in BAI during this period can be considered a reliable indicator of an actual growth decline (Peñuelas et al., 2008).

BAI was calculated from the bark to the pith, using DBH values measured in the field, from which the thickness of the bark, determined as a function of the DBH of each tree, was subtracted (Perron, 1985). For each plot, we then used the individual BAI annual data from all usable cores to create a plot-level BAI time series, calculated as the median of

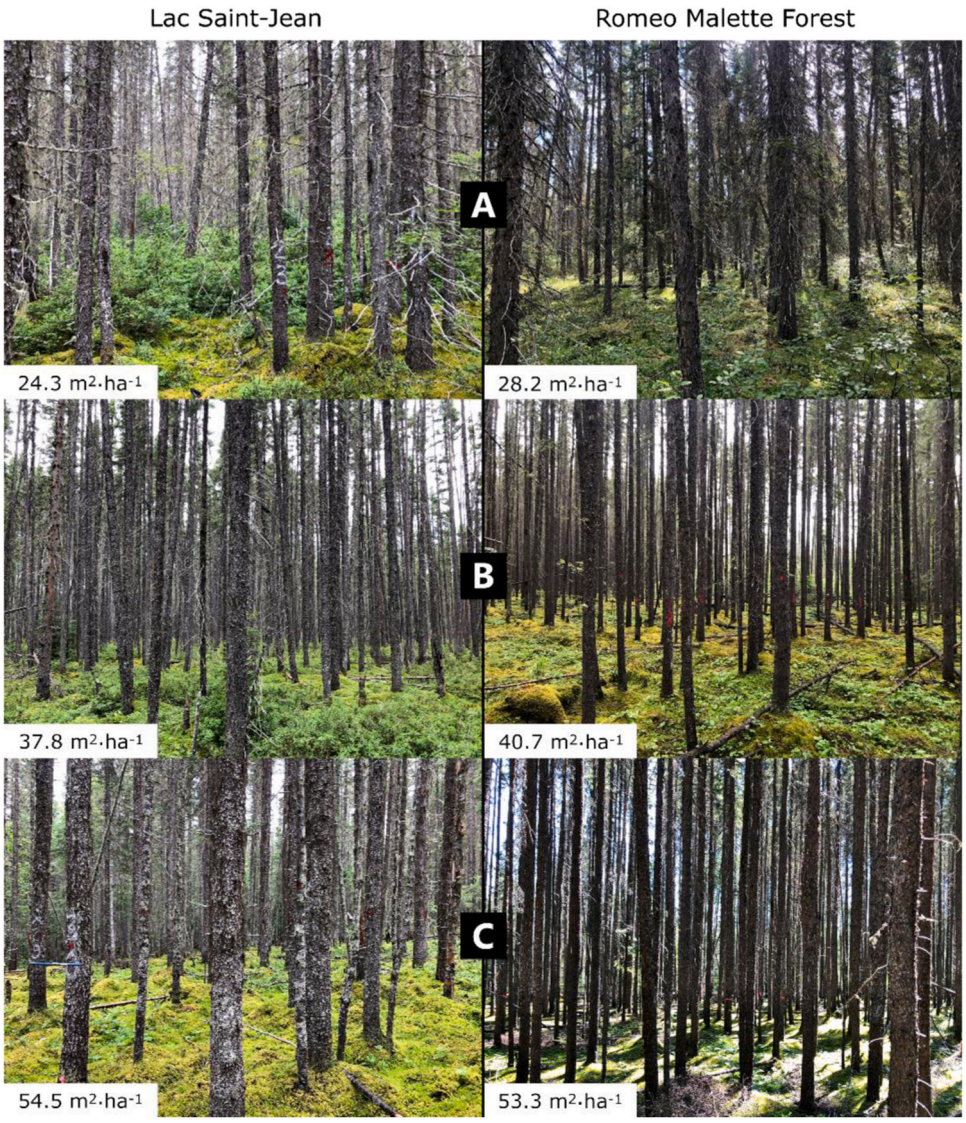

Fig. 4. Illustration of typical ground plots in the two study sites at LSJ and RMF, representing stands of low (A), medium (B), and high (C) basal area at each site.

the individual annual BAI. As high proportions of the stems were cored in each plot (35.1% on average), and sample trees were randomly selected among all trees of the plot, these median time series were deemed representative of the annual BAI of the median tree in each plot (Babst et al., 2018; Nehrbass-Ahles et al., 2014). The age of the stands was determined using the median of the number of rings counted on the discs collected at the stump of six trees in each plot.

2.4. Quantification of the decline in basal area increment

To quantify the growth decline sustained at each plot due to NSR disturbances, years 2011–2021 were used as the decline period and years 2000–2010 were used as a reference period of prior growth when BAI was relatively stable in all plots. The duration of the selected periods was determined considering the timing of the observed growth declines, and because it was sufficiently long to limit the influence of isolated low or high growth years, but short enough to avoid the influence of stand development and competition (Altman, 2020; D'Orangeville et al., 2018). This interval also corresponds approximately to the update interval of traditional forest inventories in this region (Coops et al., 2023; Gillis et al., 2005).

For each plot, we then calculated the median of the annual tree-level BAI, hereafter referred to as median growth rate, during both the reference and decline periods. The magnitude of the change in median growth rate between the two periods (hereafter referred to as decrease in growth rate) was calculated using Eq. 1. The percentage growth change between preceding and subsequent 11-year median BAI (hereafter referred to as growth decline), was calculated using Eq. 2, adapted from Nowacki and Abrams (1997).

$$\mathrm{d}BAI = BAI_{\mathrm{reference}} - BAI_{\mathrm{decline}} \tag{1}$$

$$\mathrm{d}BAI\mathrm{r} = 100 \cdot \frac{BAI_{\mathrm{reference}} - BAI_{\mathrm{decline}}}{BAI_{\mathrm{reference}}} \tag{2}$$

Where d*BAI* is the absolute difference between the median plot-level BAI in mm^2yr^{-1} over the 11-year reference ($BAI_{\mathrm{reference}}$) and decline (BAI_{decline}) periods, and d*BAI*r is the percentage change in BAI between the two consecutive periods.

Severe declines in annual BAI during the mature phase of growth are likely attributable to stressors, disturbances or senescence (LeBlanc, 1990; Peñuelas et al., 2008). In this study, we identified a threshold for severe growth declines by examining the historical range of variation in the BAI time series, considering consecutive 11-year periods. Various thresholds, either in standard deviations or percentiles, has been proposed to detect either growth releases or growth declines (e.g. Brienen

et al., 2010; Moreau et al., 2020; Trotsiuk et al., 2018) as well as growth extremes (e.g. Gazol et al. 2015; Romagnoli et al., 2018). In this study, a growth decline was considered severe if it exceeded the 95th percentile of all relative changes in median BAI between consecutive 11-year periods from 1950 to 2021. The 95th percentile is in the higher range of the thresholds reported in the abovementioned studies and was deemed appropriate considering the extent of the analysed period and the need to preserve enough observations in each category for the subsequent statistical analysis. For the determination of this threshold, the relative change in BAI was preferred to the absolute change in BAI to account for the initial variability in growth rates observed between the time series. The determination of the threshold was done by first calculating the periodic median BAI for each plot from 1950 to 2021 in subsequent, non-overlapping moving windows of the same length of the reference and decline periods described above (i.e. 11 years). The relative change in median BAI between all consecutive periods (i.e., between the first 11 years starting in 1950 and the subsequent 11 years of growth) was then calculated. The moving windows were displaced in yearly steps until the last complete period, which corresponded to that used for d*BAI* and d*BAIr* calculations (Eqs. 1 and 2). The 95th percentile of all historical relative BAI changes corresponded to a change of 23.7% in BAI between two consecutive periods. Plots for which the decrease in median growth rate between the reference and decline periods exceeded this threshold were identified as having sustained a severe growth decline.

2.5. Landsat composites, vegetation indices and derived predictor variables

Annual, gap-free, best-available pixel composites (BAP; White et al., 2014) were generated over each study site from 2000 to 2021. Integrating surface reflectance images from Landsat 5 Thematic Mapper (TM), Landsat 7 Enhanced Thematic Mapper Plus (ETM+), and Landsat 8 Operational Land Imager (OLI) sensors, these composites are created by selecting the optimal pixel for each year based on the proximity to a target date, distance to clouds and cloud shadows, atmospheric quality, and sensor-specific characteristics. Data gaps were subsequently infilled in cases where a valid annual observation was lacking for a given pixel (Hermosilla et al., 2015a; White et al., 2014). Composites were exclusively composed of Landsat scenes with less than 70% cloud cover, captured between July 1st and August 30th of each year.

Time series of vegetation indices (VI, Table 1) spanning the 2000–2021 period were calculated from the annual BAP composites. Insect defoliation, drought and other sources of stress will affect foliage coloration, density, or abundance, resulting in changes in the spectral reflectance of the canopy (Asner,1998; Coops,2015; Torresan et al., 2021). The Normalised Difference Vegetation Index (NDVI; Tucker, 1979) is a normalised difference of the near-infrared (NIR) and red Landsat bands. Photosynthetically active vegetation exhibits a high reflectance in the near-infrared region of the spectrum, but a very low reflectance in the red region of the spectrum. NDVI is a well-established indicator of the amount of photosynthetically active vegetation and has been used to monitor forest growth and mortality at both large and local scales in a variety of forest ecosystems (Beck and Goetz, 2011; Foster et al. 2022; Girardin et al., 2016). The Normalised Burn Ratio (NBR; Key and Benson, 2006) was derived from the near-infrared (NIR) and second shortwave-infrared (SWIR2) Landsat bands. Photosynthetically active vegetation shows a considerably lower reflectance in the shortwave infrared regions than in the NIR region compared to non-photosynthetic or dry vegetation (Asner, 1998). Changes in NBR are associated to changes in the amount of photosynthetically active vegetation, which have made this index useful in detecting and assessing the severity of both stand-replacing and non-stand replacing disturbances such as partial harvests and insect defoliation (Kennedy et al., 2010; Morin-Bernard et al., 2023a; 2023b). The Wetness component of the Tasseled Cap transformation (TCW; Crist,1985) incorporates information from six Landsat bands through an orthogonal transformation. TCW has been successfully employed to estimate forest structural attributes, detect declining stands, and estimate forest growth rate in the absence of disturbances (Czerwinski et al., 2014; Matasci et al., 2018, Morin-Bernard et al., 2023a; 2023b).

Table 1
Vegetation indices and related equations calculated from Landsat composite time series.

Vegetation index	Equation	Reference
Normalised Difference Vegetation Index (NDVI)	= (NIR – Red) / (NIR + Red)	(Tucker, 1979)
Normalised Burn Ratio (NBR)	= (NIR – SWIR2) / (NIR + SWIR2)	(Key and Benson, 2006a)
Tasseled Cap Wetness (TCW)	= 0.0315 * Blue + 0.2021 * Green + 0.3102 * Red + 0.1594 * NIR – 0.6806 * SWIR1 – 0.6109 * SWIR2	(Crist, 1985)

The annual values of each vegetation index were subsequently averaged over a 3 ×3 pixel window centred on the location of each of the 52 sample plots. Two categories of predictors were derived from the VI time series i.e., 1) the slope of the VI values during the 2000–2021 period, hereafter referred to as the VI slope, and 2) the difference in the median VI values (dVI) between the reference and decline periods (2000–2010 and 2011–2021, respectively). The VI slopes were determined using the Theil-Sen slope estimator (Sen, 1968; Theil, 1950), which limits the influence of outliers and noise, commonly encountered in satellite imagery time series.

2.6. Topographic predictor variables

The severity of NSR disturbance can be spatially heterogeneous and may be influenced by site characteristics and topography (Bouchard and Auger, 2014; Isaacs et al., 2014; Mamet et al., 2015). To evaluate the influence of site characteristics on the severity of NSR disturbances, we obtained surface topography information from ALS data, providing detailed wall-to-wall information on surface topography (Bufton et al., 1991; Liu, 2008; Mallet and Bretar, 2009). We used the normalised point cloud data from the ALS acquisitions conducted at each study sites to generate a digital elevation model at a 5-m resolution, from which the slope and aspect were calculated using the *terra* package (Hijmans et al., 2022) in the R programming environment. We performed sine and cosine transformations of aspect to derive two predictor variables: eastness and northness. We also calculated the topographic wetness index (TWI; Beven and Kirkby, 1979) at a 5-m resolution using the R implementation of the SAGA geographic information system (Conrad et al., 2015). The values of the topographic variables were then extracted and averaged over the 400 m^2 footprint of the ground plots.

2.7. Statistical modelling process

We implemented a two-stage modelling approach in which we first used a logistic regression model to classify the plots as either having a severe growth decline or not based on the dendrochronological summaries at the 52 plots. We then used ordinary least square regression (OLS) to predict the magnitude of the growth decline as an absolute change in BAI at the 29 plots that had sustained a severe growth decline. To develop the models at each stage, we relied on a model-selection procedure based on the Akaike information Criterion corrected for small samples (AICc), since it allows a balance between goodness of fit and model complexity, favouring the transferability of the model (Ranganathan et al., 2017). Model selection was implemented using the AICcmodavg R package (Mazerolle, 2020).

We used an identical model-selection procedure for both the logistic and the OLS regression models. To account for the presence of multicollinearity among predictors, we only tested combinations of predictors for which the variance inflation factor (VIF; Zuur et al., 2010) was less

than 2. At each step of the model-selection process, intercept-only models were also included among the candidates to ensure the most parsimonious model performed better than a simple average. For each candidate logistic regression model, the existence of a linear relationship between continuous predictor variables and the logit of the outcome was verified visually, and the absence of highly influential outliers was confirmed. Graphical methods, as well as the Shapiro-Wilk normality test and Verbyla's test for heteroscedasticity (Shapiro and Wilk, 1965; Verbyla, 1993), were used to verify assumptions for the OLS regression candidate models.

In a first step of the model selection process, we selected the best combination of Landsat-derived predictors from a set of candidates (Table 2). We then separately identified the best set of ALS-derived topographic predictor variables from a list of candidates (Table 2). We retained the set of variables with the lowest AICc value in both categories (i.e. Landsat-derived variables and ALS-derived topographic variables), for the development of comprehensive candidate models. In each category of predictors, models with small differences in AICc values (i.e., $\Delta AICc < 2$) compared to the best-ranked candidate were also retained. Comprehensive candidate models were then generated by combining the best sets of predictors from the two categories, ensuring VIF values were < 2. To assess whether the addition of topographic variables resulted in decreased AICc values compared to a model based exclusively on Landsat data, the best-performing candidate model containing only Landsat-derived predictors was also included. Both the final logistic and OLS models were selected from the set of comprehensive candidate models, with selection determined by the model with the lowest AICc value. The sample size was insufficient to split the data into training and testing dataset. Model accuracy was thus assessed using *k*-fold cross-validation as well as by applying the trained model on the entire dataset. Considering our limited sample size, we divided the dataset into five folds to ensure a minimal number of observations in the hold-out sample, which has been found to be critical in providing a reliable assessment of the predictive power of the model (e.g. Fassnacht et al., 2014). To account for a potential increase in bias and the variability of the estimates, the cross-validation process was repeated a hundred times (Kim, 2009; Rodriguez et al., 2009). The relative importance of the predictors included in the final logistic regression model was determined by calculating the drop contribution in the Tjur's coefficient of determination (Tjur, 2009) for each variable.

2.8. Application of the models to both study sites

The logistic and OLS models, respectively predicting the probability of a severe growth decline, and the magnitude of the growth decline, were then sequentially applied to make predictions throughout both study sites. To identify the area of model application (i.e. black spruce dominated stands within the study sites) over which predictions of the probability of a severe growth decline would be generated, we used data from the Quebec and Ontario FRIs for species composition (Bilyk et al., 2021; MRNF, 2022), and the abovementioned ALS-derived forest attributes layers for stand structural attributes. We first used the FRI information to select only softwood dominated stands where black spruce accounted for more than 70% of the basal area. Then, we applied an additional filtering to retain only areas where the values of canopy coverage, density, height, basal area, and mean quadratic DBH—as extracted from the ALS-derived forest attribute layers —were within the range of the same attributes measured over the plots used in model development, allowing a tolerance of ±5%. The OLS model was applied exclusively on areas where the probability of a severe growth decline predicted by the logistic regression model was $\geq$ 50%. To better understand how much the defoliation caused by the spruce budworm may have contributed to the observed growth declines, we conducted an additional analysis to determine if there was a significant difference in the cumulative number of years of defoliation during the current outbreak in areas where a severe growth decline was predicted compared to areas where a severe growth decline was not predicted. For our analysis, we extracted the cumulative number of years of defoliation from Fig. 2 over each 30 ×30 m cells on which logistic model predictions were generated. We then carried out an analysis of variance to look for significant differences in defoliation data between cells where the predicted probability of severe growth decline was $\geq$ 50% compared to areas where the predicted probability was $<$ 50%.

Table 2
Candidate models including either Landsat-derived spectral or ALS-derived topographic variables tested in the logistic and OLS model selection procedures. TCW is the Tasseled Cap Wetness, NBR is the Normalised Burn Ratio, NDVI is the Normalised Difference Vegetation Index and TWI is the Topographic Wetness Index. The letter d refers to the difference in the median vegetation index value between the reference (2000–2010) and decline (2011–2021) periods.

Landsat-derived variables		ALS-derived topographic variables	
Model ID	**Variables**	**Model ID**	**Variables**
1	TCW slope	1	Elevation
2	TCW slope + dNDVI	2	Elevation + TWI
3	NBR slope	3	Elevation + Slope
4	NBR slope + dNDVI	4	Slope
5	NDVI slope	5	TWI
6	NDVI slope + dNBR	6	Slope + Northness + Eastness
7	NDVI slope + dTCW	7	Northness + Eastness
8	dNDVI	8	Intercept only
9	dNBR		
10	dTCW		
11	Intercept only		

3. Results

3.1. Compositional, structural attributes and age of the ground plots

The forest structural attributes, year of origin, and species composition of the ground plots established as part of this study are presented in Table 3. Stand age varied between 76 and 114 years at the time of sampling in 2021, as determined from the discs collected at the base of the stems on six trees per plot. Fig. 4 shows typical representations of stands of low, medium, and high basal area encountered at the LSJ and RMF sites.

3.2. Changes in basal area increment between the reference and decline periods

Fig. 5 shows the mean BAI trends from 1950 to 2021 for each study site, calculated as the average of the tree-level annual BAI calculated at each plot. On average, BAI was higher at the LSJ site throughout the observation period until 2021, when values at both sites reached comparable values (Fig. 5). At the LSJ site (28 plots, 848 trees), the median growth rate during the reference period (period A in Fig. 6) ranged from 124.3 to 321.7 mm^2yr^{-1} depending on the plot, with an average of 219.16 mm^2yr^{-1}.

For plots located at the RMF site (24 plots, 690 trees), the median growth rate during the reference period had minimum, maximum, and average values of 108.0, 245.4 and 162.6 mm^2yr^{-1}, respectively. The average relative growth declines between the reference and decline periods were 27.7% at the LSJ site and 29.9% at the RMF (Fig. 6). At the LSJ site, only one plot had a slightly positive change in BAI (+ 0.2%), while remaining plots showed decreases in BAI that reached 65.5% in the most affected plot. At the RMF site, the relative decrease in BAI between the two periods ranged from 2.2% to 52.4%. A total of 29 plots (thirteen at the LSJ site and sixteen at the RMF site) reached the threshold determined for severe growth declines (i.e. 23.7% decrease in BAI), corresponding to 55.8% of the plots included in the study.

Table 3
Summary of stand attributes for the ground plots established at the Lac Saint-Jean (LSJ) and Romeo Malette Forest (RMF) sites, calculated from the field measurements in 400 m^2 circular plots.

	Lac Saint-Jean	Romeo Malette Forest
Year of origin		
Average	1930	1923
Min	1913	1908
Max	1946	1939
Basal area (m^2 ha^{-1})		
Average	39.3	40.4
Min	24.3	28.2
Max	54.5	58.0
Stem density (stem ha^{-1})		
Average	2286	2872
Min	1050	1225
Max	3525	4275
Quadratic Mean DBH (cm)		
Average	15.2	13.6
Min	11.9	12.0
Max	18.4	18.1
Composition (% BA)		
Black spruce		
Average	96.9	97.1
Min	77.2	79.6
Max	100.0	100.0
Jack Pine		
Average	5.9	4.6
Min	1.3	0.4
Max	22.8	12.7
Balsam fir		
Average	1.1	1.2
Min	0.1	0.1
Max	4.4	5.8
Deciduous		
Average	1.8	3.6
Min	0.9	1.9
Max	3.1	5.2

3.3. Probability of a severe growth decline

The inclusion of both Landsat-derived spectral and ALS-derived topographic variables in the logistic regression model increased model performance compared to the best-ranked models that included only predictors from a single category and resulted in lower AICc values. The best-performing comprehensive model included the slope of the TCW, as well as the elevation, and the TWI as predictors (Table 4).

The selected model predicting the probability of severe growth decline (i.e. Model ID 7) achieved an accuracy of 80.8% when the model was applied to the full dataset (i.e., all 52 plots). The overall accuracy was slightly lower when calculated using repeated five-fold cross-validation, at 79.2%. The confusion matrix of model predictions on the entire dataset is presented in Table 5, and the individual effects of the predictors included in the model are shown in Fig. 7. The producer's accuracy was 86.2% for plots with no severe decline and 73.9% for plots with severe decline. The values of user's accuracy for these classes were 80.7% and 66.7%, respectively. Errors of commission were 19.1% for plots with no severe decline and 19.4% for plots with severe decline. The corresponding errors of omission for these classes was 26.1% and 13.8%, respectively. Compared to the best-ranked model, which included only Landsat-derived variables (Model ID = 1), the inclusion of topographic variables increased the overall accuracy of the final model by 11.6% (80.8 vs 69.2) when measured on the full dataset and reduced the AICc by 6.61 (Table 4). The Tjur's coefficient of determination of the final model was 0.47. Removing either the slope of the TCW, the elevation or the TWI from the predictor variables decreased the Tjur's coefficient of determination by 0.14, 0.08 and 0.06, respectively.

A steeper negative slope of the TCW was associated with an increased probability of a severe decline in BAI between the two periods (Fig. 7). Areas located at higher elevation had a lower probability of having sustained a severe decline in BAI, while higher values of the TWI were associated with a higher probability of a severe decline in BAI.

3.3.1. Application of the logistic regression model to the study sites

The probability of a severe growth decline was mapped wall-to-wall over the two study sites (at a 30 m spatial resolution), for forested areas where the structure and composition were similar to those of the stands used for model development (i.e., $\geq$ 70% of BA in black spruce, ALS-derived structural attributes within the range presented in Table 3 $\pm$ 5%). At the LSJ site, the model was applied on a total area of 32,841 ha (Fig. 8A), and 29,454 at the RMF site (Fig. 8B).

Across the LSJ site, 7432 ha, or 22.6% of the area, had a probability of severe growth decline of 50% or more, with a median predicted probability of 8.8%. At the RMF site, 16,978 ha (57.6%) of the model application area had a probability of severe growth decline of 50% or more. Although the proportion of the area with a predicted probability of severe growth decline was considerably higher at the RMF site, the

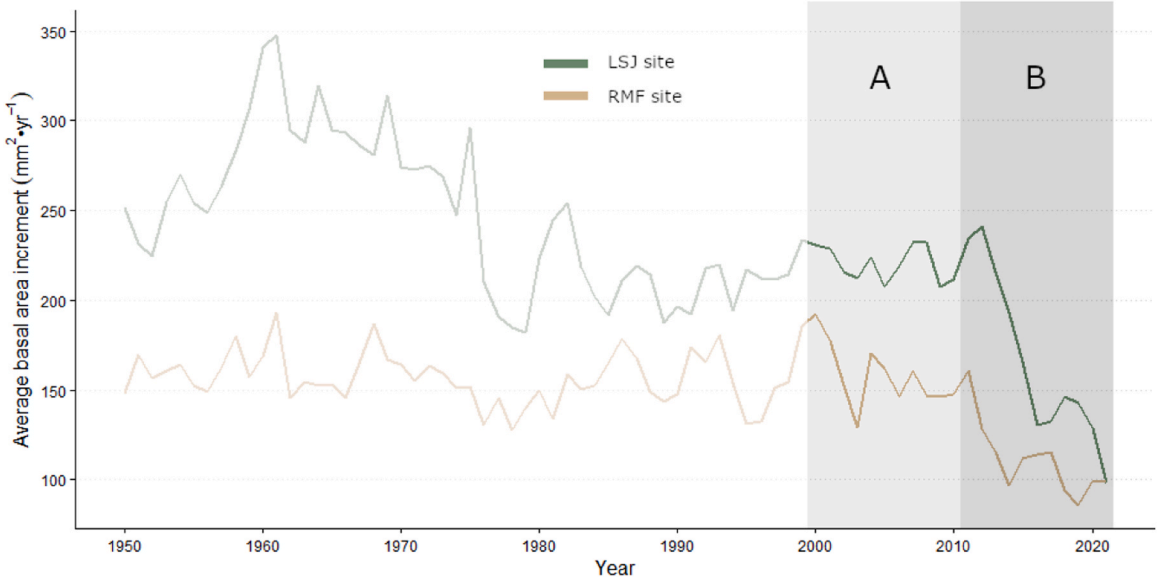

Fig. 5. Site-level BAI chronologies from 1950 to 2021, built by averaging the BAI calculated at each plot. Shaded areas indicate the reference (A) and decline (B) periods.

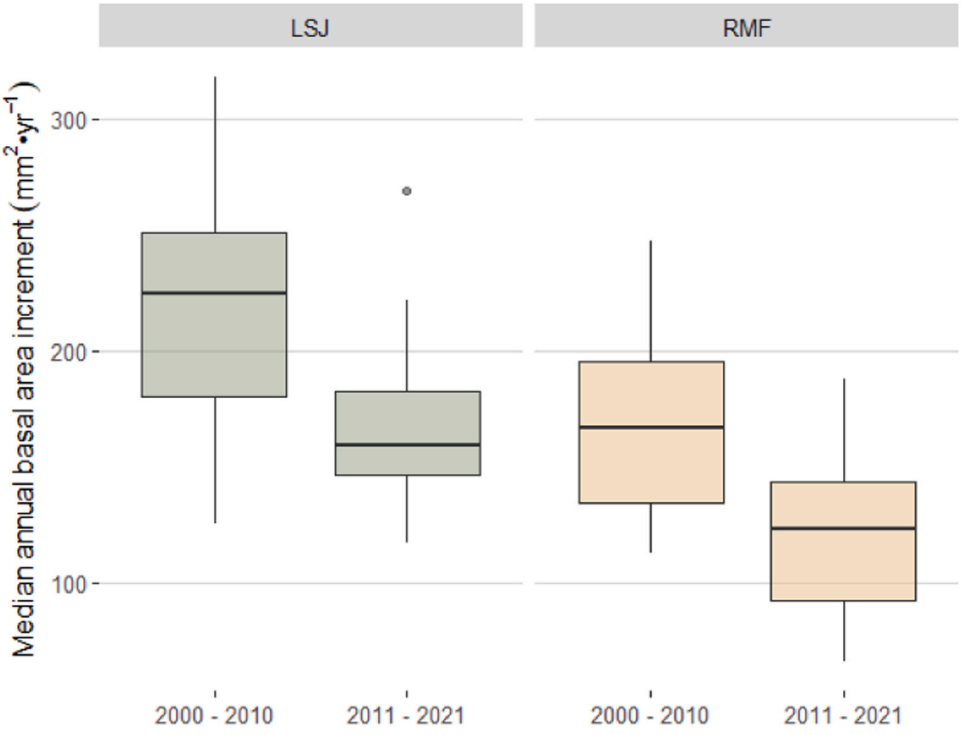

Fig. 6. Median BAI growth rate of the plots located at the LSJ and RMF sites during the reference (2000–2010) and the decline (2011–2021) periods.

Table 4
Ranking of the candidate logistic regression models for the prediction of the occurrence of a severe growth decline. AICc is the Akaike Information Criteria, corrected for small sample sizes, with delta AICc (ΔAICc), relative model likelihood (Mk), and AICc weight (Wt_i).

Model ID	Model name	AICc	ΔAICc	Mk	Wt_i
7	TCW slope + Elevation + TWI	51.82	0.00	1.00	0.35
5	TCW slope + Elevation + Slope	52.80	0.98	0.61	0.21
3	TCW slope + Elevation	53.02	1.19	0.55	0.19
8	TCW slope + dNDVI + Elevation + TWI	54.27	2.45	0.29	0.10
6	TCW slope + dNDVI + Elevation + Slope	55.25	3.43	0.18	0.06
4	TCW slope + dNDVI + Elevation	55.36	3.54	0.17	0.06
1	TCW slope	58.43	6.61	0.04	0.01
2	TCW slope + dNDVI	60.14	8.32	0.02	0.01
9	Intercept only	73.47	21.65	0.00	0.00

Table 5
Confusion matrix for the predictions of the occurrence of severe growth decline using the final logistic regression model (Model ID 7) applied to the 52 plots.

	Observed	
Predicted	No severe decline	Severe decline
No severe decline	17	4
Severe decline	6	25

proportion of the model application area where the predicted probability exceeded 90% was lower at the RMF than at the LSJ site, with proportions of 5.8 and 10.2%, respectively.

Within the LSJ site, areas mapped as having experienced a severe growth decline (i.e., ≥ 50% probability according to predictions of the logistic regression model) had undergone defoliation for a significantly greater ($p < 0.001$) number of years than areas where the predicted probability of severe growth decline was < 50%, with average years of defoliation of 3.9 and 2.1, respectively. At the RMF site, the difference between the two categories of stands was also significant ($p < 0.001$), although the difference between the average number of years of defoliation in both areas of severe growth decline (0.7 years) and areas with no severe growth decline (0.4 years) was considerably smaller.

3.4. Magnitude of the decrease in BAI

The best-ranked model predicting the magnitude of decrease in BAI between the reference and decline periods included a single Landsat-derived predictor, which was the slope of the TCW index (Table 6). The addition of ALS-derived topographic variables did not increase model performance, although two candidate models including topographic variables had only slightly higher AICc values compared to the best-ranked model (Table 6).

The best-ranked model had an $R^2 = 0.70$ ($p < 0.01$, RMSE = 23.67 mm^2yr^{-1}) after five-fold cross-validation repeated a hundred times and a R^2 of 0.71 ($p < 0.01$, RMSE = 24.70 mm^2yr^{-1}) when calculated on data from all plots. Fig. 9 shows the actual versus predicted decrease in growth rate for the twenty-nine plots that sustained a severe growth decline between the two sub-periods.

A steeper TCW slope during the 2000–2021 period was associated with a larger decrease in BAI between the reference (2000–2010) and decline (2011–2021) periods (Fig. 10).

3.4.1. Application of the OLS model to the study sites

Predictions of the magnitude of the decrease in BAI between the reference and the decline periods were generated in all areas where the predicted probability of a severe growth decline reached 50% or more. At the LSJ site, the median predicted decrease in growth rate for these pixels was 95.3 mm^2yr^{-1}, with a 5th percentile of 42.9 mm^2yr^{-1} and a 95th percentile of 191.5 mm^2yr^{-1}. The median predicted decrease in growth rate at the RMF site was lower at 64.4 mm^2yr^{-1}, with 5th and 95th percentiles of 36.7 and 101.7 mm^2yr^{-1}, respectively. Fig. 11 shows the predicted growth decline in the areas of the two study sites where the highest probabilities of severe growth decline were found. Areas with the most severe declines appeared to be spatially clustered. Compared to the LSJ site, a larger area was predicted to have experienced a severe

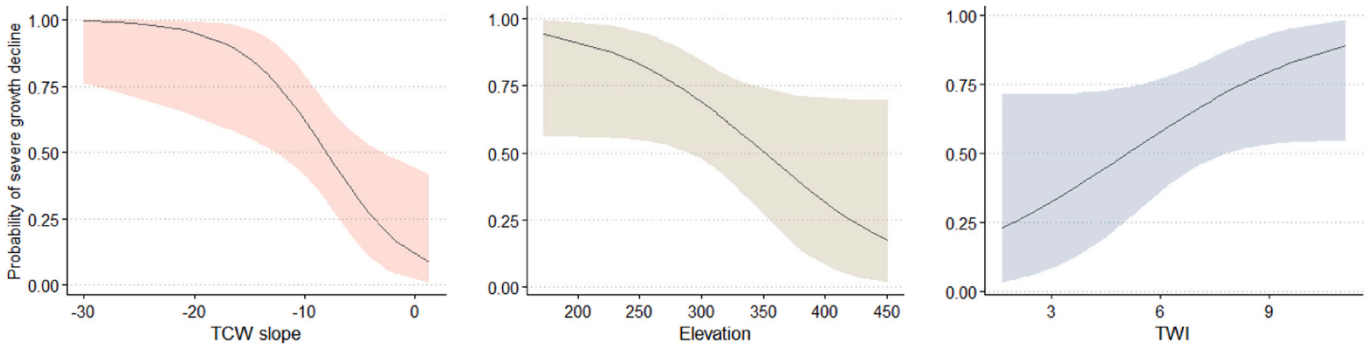

Fig. 7. Model predictions and unconditional 95% confidence intervals for the variables included in the best-ranked model predicting the probability of a severe growth decline between 2000 and 2010 and 2011–2021.

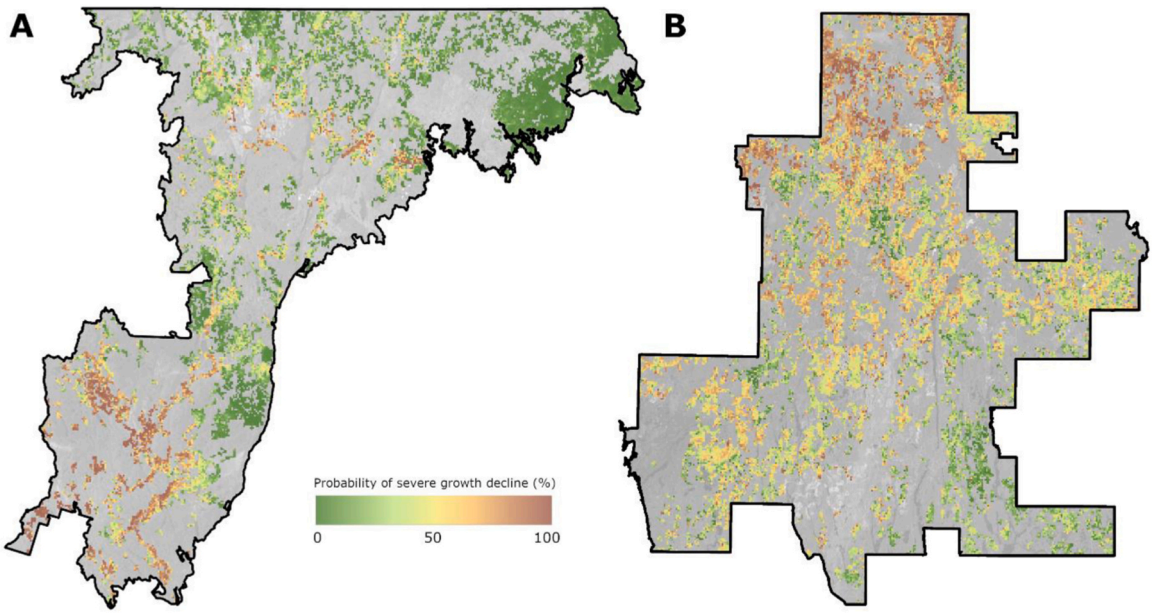

Fig. 8. Predicted probability of severe growth decline between the reference (2000–2010) and decline (2011–2021) periods at the LSJ (A) and RMF (B) sites. For visualization purposes, the 30 m pixels were aggregated into 200 m pixels showing the average probability value.

Table 6
Ranking of the candidate OLS regression models for the prediction of the magnitude of the growth decline. AICc is the Akaike Information Criteria, corrected for small sample sizes, with delta AICc (ΔAICc), model likelihood (Mk), and AICc weight (Wt_i).

Model ID	Model name	AICc	ΔAICc	Mk	Wt_i
1	TCW slope	272.77	0.00	1.00	0.24
3	TCW slope + Slope	272.93	0.16	0.92	0.22
5	TCW slope + TWI	272.95	0.18	0.91	0.22
2	TCW slope + dNDVI	273.65	0.88	0.64	0.15
6	TCW slope + dNDVI + TWI	274.67	1.90	0.39	0.09
4	TCW slope + dNDVI + Slope	275.11	2.34	0.31	0.07
7	Intercept only	306.68	33.91	0.00	0.00

growth decline in the RMF site, but the magnitude of the decline was generally lower in the latter at the RMF site.

4. Discussion

Whereas significant progress has been made towards detecting and assessing the severity as well as the levels of mortality attributable to NSR disturbances (Coops et al., 2020; Morin-Bernard et al., 2023a; 2023b; Mulverhill et al., 2023; Senf et al., 2015), our study focused on signs of growth decline, which may be indicators of imminent mortality (Anderegg et al., 2019; Kéfi et al., 2013; Mamet et al., 2015). Our results showed that a substantial growth decline occurred in certain areas of both study sites over the 2011–2021 period. Although the results presented in this study do not allow us to quantify the relative impact of defoliation and drought on the observed growth declines, the results provide valuable information to forest managers who need spatially explicit information on the current state of forests in order to plan appropriate management interventions.

4.1. Integration of landsat time series and tree-ring data

The predictive ability of the models developed in this study and the correlations between the BAI declines and the selected predictors variables confirm that Landsat time series can be utilised to quantify growth declines in black spruce stands due to NSR disturbances, thus fulfilling the main objective of this study. While previous studies focused on the characterisation of the temporal connection between tree-rings and Landsat time series data and on assessing changes in growth trends (e.g. Babst et al., 2010; Bonney and He, 2021; Decuyper et al., 2020; Lopatin et al., 2006; Vicente-Serrano et al., 2016), our study exploits the correlations between these sources of data to generate spatially explicit predictions of changes in growth rates in a measurement unit (i.e. BAI)

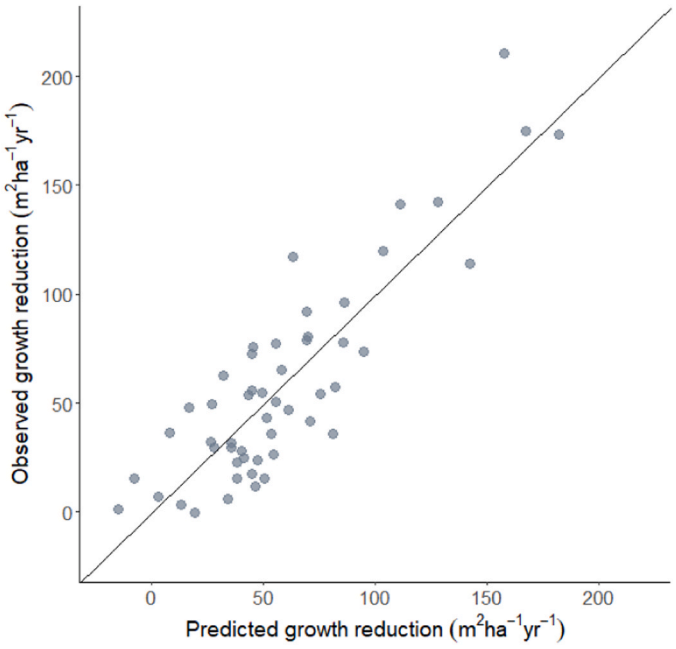

Fig. 9. Actual versus predicted decrease in BAI (mm^2yr^{-1}) for the twenty-nine plots that sustained a severe growth decline between the reference (2000–2010) and decline (2011–2021) periods. The solid line indicates the 1:1 ratio.

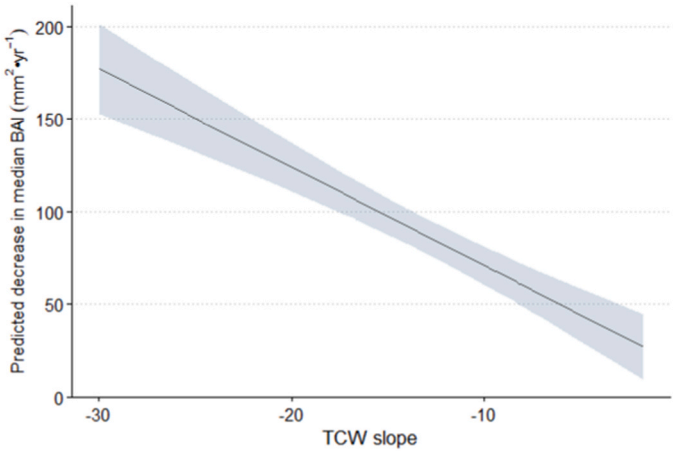

Fig. 10. Model predictions and unconditional 95% confidence interval for the TCW slope, which was included in the best-ranked OLS model to predict the magnitude of the change in BAI.

that is relevant for forest management and silvicultural decision-making. In a previous study, Morin-Bernard et al., (2023a); (2023b) used Landsat time series to predict the annual net basal area growth of undisturbed coniferous stands, based on data from permanent sample plots. One limitation of using permanent sample plot data for growth assessment is the limited temporal resolution of these datasets, with field measurements typically conducted every 5 or 10 years (Coops et al., 2023; Gillis et al., 2005). The annual resolution of tree-ring data allows for targeting of specific periods corresponding to disturbance events or adverse climatic conditions. The considerable number of increment cores collected as part of the provincial and national inventory programs, as well as datasets available from the International Tree-Ring Data Bank (Grissino-Mayer and Fritts, 1997; Zhao et al., 2019) and from the Canadian Tree Ring Database (CFS-TRenD; Girardin et al. 2021) constitute precious and relatively untapped sources of data that could be employed to apply a similar approach across a wide variety of forest types in Canada and around the world.

The quality of tree ring data in terms of sampling and standardisation, however, remains a challenge. Dendrochronological analysis, traditionally used to reconstruct past climate, usually involves the sampling of dominant trees only, because they show similar responses to climate (Babst et al., 2018; Biondi, 1999; Nehrbass-Ahles et al., 2014). This causes an overestimation bias in estimates of forest growth at the stand level, since the growth of intermediate and supressed trees is not considered (Babst et al., 2014; Klesse et al., 2016; Nehrbass-Ahles et al., 2014). The number of cores collected at each site can also be insufficient to capture the local variability in growth rates and responses to disturbances (Nehrbass-Ahles et al., 2014). Finally, some of these tree ring datasets do not include the raw ring-width measurements, but rather a standardised ring-width index, obtained after applying some form of detrending to the tree-ring data (Biondi and Qeadan, 2008; Sullivan et al. 2016). Although this standardisation removes low-frequency signals related to variations in stem size, cambial age, and development stages (Biondi and Qeadan, 2008; Guibal and Guiot, 2021), it prevents the calculation of an actual growth rate and the comparison of growth rates at different times (Klesse et al., 2016; Sullivan et al., 2016). Converting the tree-ring widths to BAI, as realised in the current study presented herein, is an appropriate approach to minimize bias when investigating trends in growth or carbon assimilation over time (Babst et al., 2018; Klesse et al., 2016; Nehrbass-Ahles et al., 2014).

4.2. *Predictor variables included in the final models*

The final logistic regression model used herein to predict the probability of severe growth decline comprises both Landsat-derived predictors associated with the trend in the canopy spectral reflectance of the stands, as well as ALS-derived topographic variables, whereas the final OLS regression model used to predict the magnitude of the decrease in BAI includes only Landsat-derived predictors.

The Theil-Sen slope of the TCW was the most important predictor in both the logistic and OLS regression models, confirming that the investigated NSR disturbances and the associated decline in growth has an impact on the spectral reflectance properties of the canopy. Previous work has shown the utility of the TCW to measure the annual net growth rate of coniferous stands in one of the sites used in the current study (Morin-Bernard et al. in press). Similarly, Czerwinski et al. (2014) used the Theil-Sen slope of the TCW to identify declining stands in a Canadian mixedwood forest. Other authors have also observed that TCW is among the most important predictors of canopy coverage and forest biomass (Matasci et al., 2018; Zald et al., 2016). The capacity of the TCW index to better capture changes in growth than the other tested indices appears to be linked to the specific weight given to each Landsat band in the TCW calculation. The general spectral response to a reduction in foliage abundance or density consecutively to a NSR disturbance involves a decrease in the NIR portion of the electromagnetic spectrum and an increase in the visible and SWIR wavelengths (Franklin et al., 2001; Healey et al., 2006). The strong emphasis of the TCW coefficients on the SWIR bands would therefore result in lower TCW values in response to reductions in canopy. In contrast, NDVI and other greenness-based indices, which are more sensitive to changes in the visible and NIR wavelengths, relate more notably to the spectral reflectance properties of chlorophyll (Asner, 1998; Tucker, 1979). Such indices easily become saturated in highly vegetated environments and are more sensitive to changes in the canopy that are not related to forest productivity (Fiore et al., 2020; Sulla-Menashe et al., 2018). This could explain, at least partially, the weak or inconsistent relationships found in previous studies between tree-ring data and Landsat-derived NDVI or Enhanced Vegetation Index (EVI) (Bonney and He, 2021; Decuyper et al., 2020; Vicente-Serrano et al., 2016).

The impact of biotic or abiotic stressors and disturbances is related to site-specific factors (Isaacs et al., 2014; Mallet and Bretar, 2009; Mamet et al., 2015), which can be captured by topographical information

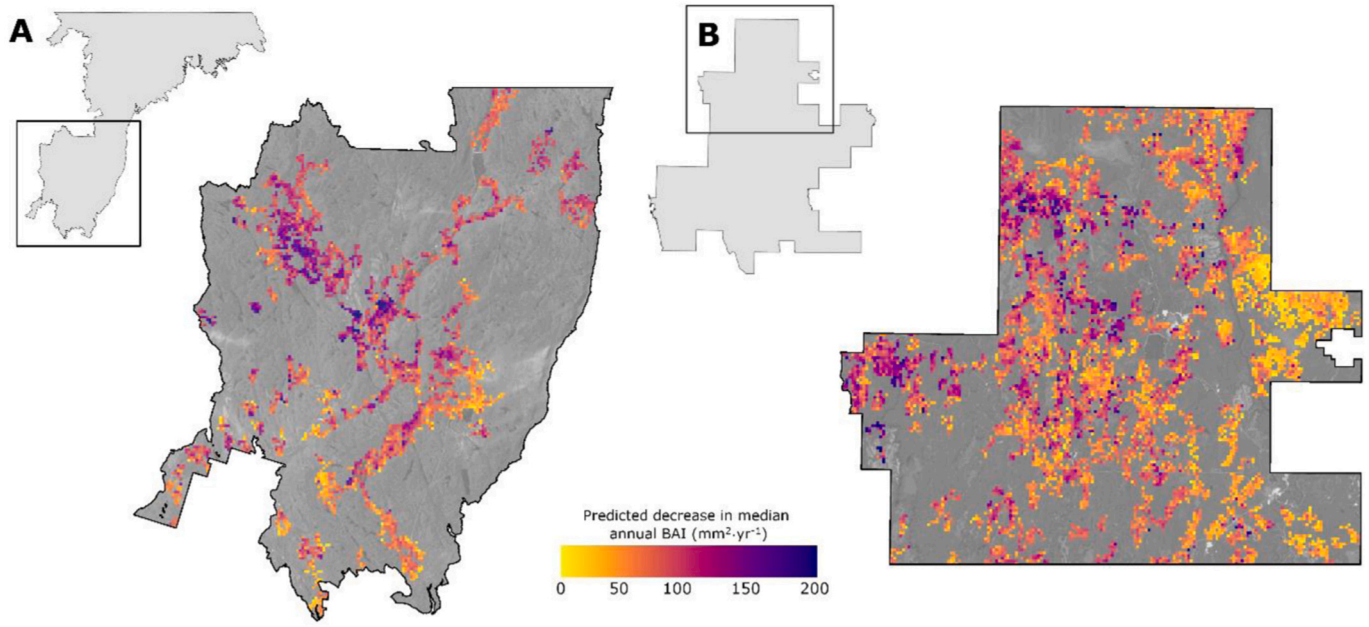

Fig. 11. Predicted decrease in median annual growth rate (BAI; mm^2yr^{-1}) between the reference (2000–2010) and decline (2011–2020) periods for sub-areas of the LSJ (A) and RMF (B) study sites that have sustained the largest declines.

obtained from ALS data. The inclusion of elevation and TWI increased the accuracy and fit of the logistic regression model predicting the probability of severe growth decline, thus addressing one of the objectives of this study. Although we did not aim to quantify the relative contribution of the two investigated NSR disturbances on the observed growth declines, the respective effect of topographical variables included in the model is consistent with findings from previous studies on both spruce budworm defoliation and drought events. The higher susceptibility to defoliation by the spruce budworm observed at lower elevations could be attributable to the effects of elevation on temperature, forest productivity, species composition, and soils (Blais, 1957; Hodkinson, 2005; Magnussen et al., 2004), although Bouchard and Auger (2014) found a low association between these characteristics and the intensity of the defoliation. The effect of drought can also be influenced by the topographic position of the stands. Although trees on the driest sites are often the most vulnerable to drought, our findings suggest the opposite. Stands at lower elevations and those with higher TWI values were more likely to experience a severe growth decline. Similar conclusions have been drawn from other studies conducted on black spruce and co-occurring boreal species in Canada. Black spruce trees situated in cooler, wetter locations were more adversely affected by drought compared to trees growing on dry sites (Walker et al., 2015; Wolken et al., 2016), a phenomenon also observed on white spruce (Lloyd et al., 2013). A common hypothesis for this is that low elevation, wet sites accumulate a high snow load compared to sites along slopes or on hilltops. This extends the period during which roots remain frozen, which impedes photosynthesis when the evaporative demand begins to increase because of warmer air temperatures (Lloyd et al., 2013; Walker et al., 2015; Wolken et al., 2016). The physiological limitation on water uptake from roots in cold soils cause these stands to be vulnerable to early season moisture deficit during warm springs, consistent with the previously reported negative response of growth to spring temperatures (Lloyd et al., 2013; Wolken et al., 2016). This seemingly higher vulnerability to drought in wet, low topographic positions may also be attributable to genetic differences, particularly those that enable certain black spruce families to better tolerate water deficits (Tan and Blake, 1997). Trees growing in consistently humid sites may exhibit fewer adaptations to drought than those growing at higher altitudes or where water stress is more frequent, although this hypothesis would require additional investigation.With respect to the impact of spruce budworm defoliation, wetter and less productive sites are at greater risk of experiencing severe growth declines during an outbreak (Payette and Delwaide, 2003; Sánchez-Pinillos et al., 2019), although others have concluded that site wetness does not have a significant influence (Bouchard and Auger, 2014; Lacey and Dech, 2012).

4.3. *Effect of NSR disturbances on changes in BAI*

The magnitude of the predicted growth declines was spatially highly variable across the study sites and raises uncertainty regarding the future of the most affected stands. Understanding the underlying causes of the variability in the observed growth declines represents a challenge considering the potential interactions between disturbance agents.

While our results do not allow us to determine the relative impact of drought events and defoliation by the spruce budworm on the observed growth declines, a comparison of model predictions with defoliation data suggests that both disturbances likely played a contributing role. Aerial defoliation survey data confirms that model predictions of tree growth decline are generally spatially coherent with the pattern of defoliation observed across the study sites. Areas that have experienced defoliation for a longer period are also, in general, those where the risk of growth decline is mapped as the highest. The cumulative number of years with defoliation was, however, lower at the RMF site, as the outbreak started only in 2015, a few years after the onset of the growth decline. We note that several plots at the RMF site were mapped as not defoliated during the aerial surveys, yet they sustained a considerable decrease in BAI. Within each study site, there was substantial variability in the number of years with defoliation, both in areas of severe growth decline and in areas where no severe growth decline was predicted by the logistic regression model. At the LSJ site, the cumulative years of defoliation in areas of severe growth decline ranged from 0 years (5th percentile) to 8 years (95th percentile), while in areas without severe growth decline, the corresponding values were 0 and 6 years. Similarly, at the RMF site, areas of severe growth decline experienced between 0 (5th percentile) and 3 years (95th percentile), while in areas without severe growth decline, the corresponding values were 0 and 2 years, respectively. These results suggest that the spruce budworm is just one of the factors contributing to the observed growth declines, which could

be explained by the combined effect of insect defoliation and drought (Bouchard et al., 2018; De Grandpré et al., 2019).

Drought conditions can impact vigour and growth for several consecutive years, persisting even when the climate becomes more humid (Kannenberg et al., 2020; Wu et al., 2018). This legacy effect of drought can emerge after a single event or through an accumulation of relatively mild droughts, which decreases the tree's resilience and make it more vulnerable to subsequent stressors (Kannenberg et al., 2020; Liu et al., 2019; Sánchez-Pinillos et al., 2022). There can also be a lag between the occurrence of drought and the impacts on growth and mortality (Anderegg et al., 2019; Itter et al., 2019; Kannenberg et al., 2020). The detrimental effects of the drought periods observed at both sites could explain why the growth decline was initiated synchronously despite the spruce budworm outbreak starting several years later at the RMF site than at the LSJ site.

4.4. Implications for the management of black spruce forests under climate change

This study is part of a wider research effort dedicated to the production of so-called living or continuous forest inventories, which rely on a combination of remote sensing data, ground-based surveys, and forest growth modelling to produce forest inventories that are precise, spatially explicit, and frequently updated (Coops et al., 2023). Our approach enables the production of spatially explicit information on the probability of severe growth declines in black spruce stands, as well as a quantification of the associated changes in BAI. The Landsat-derived predictor included in both the logistic and OLS regression models captured the associated changes in the canopy spectral reflectance response. While the detection and mapping of the severity of NSR disturbances such as drought and insect defoliation is increasingly common (Coops et al. 2020), the current study is among the first to link these disturbances to a direct measure of tree growth using remotely sensed data and to generate predictions over areas equivalent to that of a forest management unit. The proposed method opens new opportunities for adopting more agile and adaptive forest management and silvicultural practices. Areas identified as the most at risk of having experienced a severe growth decline could be targeted for silvicultural actions aimed at enhancing the resistance and resilience of the stands, or could be prioritized for harvest in order to limit the risks of losses due to imminent mortality (Achim et al., 2022; Moreau et al., 2022), which could also result in the increased risk of fire ignition under certain circumstances (James et al., 2017).

Quantifying the magnitude of the growth decline caused by NSR disturbances also provides valuable information required to update growth and yield projections in a forest management unit. This information would allow adjustments of harvest levels to account for the observed losses, which were not necessarily foreseen by the current growth and yield models. Additionally, such data could enable near real-time adjustments of carbon exchange models with the atmosphere and improve the calculation of the carbon balance, which is inevitably impacted by such growth reductions (Boisvenue and White, 2019; Klesse et al., 2016; Wang et al., 2021).

Several challenges remain to be addressed for an operational implementation of the approach. The current study was conducted on a single, relatively homogeneous forest type, and further work is needed to verify the transferability of the models to other forest types, or to develop models applicable over a larger proportion of the stands composing the boreal forest. Additional work is also necessary to investigate the influence of the time window used to measure the change in growth from the tree rings. In this study, an 11-year window was utilised, which corresponds approximately to the update interval of traditional forest inventories (Coops et al., 2023; Gillis et al., 2005). The possibility of using shorter intervals could also be explored as it would allow for the earlier detection of decline and the more rapid implementation of targeted interventions. The next steps also involve estimating volume and total aboveground biomass losses, which are fundamental units of forest yield and productivity. The increasing availability of repeated LiDAR acquisitions, enabling fine-scale mapping of forest attributes, offers the opportunity to achieve this objective.

5. Conclusion

This study demonstrated the usefulness of Landsat data to estimate the probability of severe growth decline as a result of NSR disturbances, namely drought and defoliation by the spruce budworm. The slope of the TCW index was the most important predictor of BAI decline. Using this index also allowed for the prediction of the magnitude of the growth decline in the most affected areas. The inclusion of ALS-derived topographic variables, specificatlly elevation and TWI, improved the accuracy of the logistic regression predicting the probability of a severe growth decline, but did not improve the performance of the OLS regression model aimed at predicting the magnitude of the change in BAI over time. Although the current study was limited to a specific forest type and condition, our results show the potential of linking a direct measure of forest growth (i.e. tree-ring data) to Landsat time series data to generate relevant information for forest management decision-making. In a context of uncertainty regarding future disturbance regimes and their impacts on timber supply and forest carbon stocks, generating spatially explicit information on changes in forest growth due to NSR disturbances could help concentrate field efforts and silvicultural interventions in the most affected or vulnerable areas.

Funding

This work was supported by the NSERC Alliance project Silva21 [NSERC ALLRP 556265-20 to A.A.]; and the NSERC Alexander Graham Bell Graduate Scholarships-Doctoral Program [CGS-D to A.M.B].

CRediT authorship contribution statement

White Joanne C.: Writing – review & editing, Supervision, Resources, Funding acquisition. **Coops Nicholas C.:** Writing – review & editing, Supervision, Resources, Funding acquisition. **Achim Alexis:** Writing – review & editing, Supervision, Project administration, Methodology, Funding acquisition, Conceptualization. **Morin-Bernard Alexandre:** Writing – original draft, Visualization, Project administration, Methodology, Investigation, Conceptualization.

Declaration of Competing Interest

The authors declare that they have no known competing financial interests or personal relationships that could have appeared to influence the work reported in this paper.

Data availability

Data will be made available on request.

Acknowledgments

We would like to acknowledge the support of the government, institutional, and industrial partners involved in the Silva21 research project, especially our collaborators from the Ontario Ministry of Natural Resources and Forestry, and Quebec's Ministère des Ressources Naturelles et des Forêts for sharing data and authorizing the collection of samples necessary for this project. We would also like to thank Chris McDonell and his team from GreenFirst Forest Products for their assistance in accessing and assembling the data required for this study and for their support in the planning and execution of the fieldwork. Additionally, we would light to acknowledge the contribution of Loic D'Orangeville for his advice regarding the sampling protocol and to Ann

Delwaide for sharing her knowledge of dendrochronology with the project team. The authors also want to thank the team that contributed to data collection in the field and their analysis in the laboratory. Special thanks to Philippe Riel, Florence Leduc, Justine Gillis, Véronique Jodoin, Sébastien Dumont, Catherine Chagnon, Tommaso Trotto, Félix Coulaud, Achille Oettli, Vincent Filion, Flavie Dubé, Pierre-Yves Normandin, and Maxime Kelleher.

References

Aakala, T., Remy, C.C., Arseneault, D., Morin, H., Girardin, M.P., Gennaretti, F., Navarro, L., Kuosmanen, N., Ali, A.A., Boucher, É., Stivrins, N., Seppä, H., Bergeron, Y., Girona, M.M., 2023. Millennial-Scale Disturbance History of the Boreal Zone, Sustainable Management (ppBoreal Forests in the Face of Climate Change. Springer International Publishing, pp. 53–87, 10.1007/978-3-031-15988-6_2M.M.GironaH. MorinS.GauthierY.Bergeron..

Achim, A., Moreau, G., Coops, N.C., Axelson, J.N., Barrette, J., Bédard, S., Byrne, K.E., Caspersen, J., Dick, A.R., D'Orangeville, L., Drolet, G., Eskelson, B.N.I., Filipescu, C. N., Flamand-Hubert, M., Goodbody, T.R.H., Griess, V.C., Hagerman, S.M., Keys, K., Lafleur, B., White, J.C., 2022. The changing culture of silviculture. For.: Int. J. For. Res. 95 (2), 143–152. https://doi.org/10.1093/forestry/cpab047.

Ahmed, O.S., Wulder, M.A., White, J.C., Hermosilla, T., Coops, N.C., Franklin, S.E., 2017. Classification of annual non-stand replacing boreal forest change in Canada using Landsat time series: a case study in northern Ontario. Remote Sens. Lett. 8 (1), 29–37. https://doi.org/10.1080/2150704X.2016.1233371.

Altman, J., 2020. Tree-ring-based disturbance reconstruction in interdisciplinary research: current state and future directions. Dendrochronologia 63, 125733. https://doi.org/10.1016/j.dendro.2020.125733.

Anderegg, W.R.L., Anderegg, L.D.L., Huang, C., 2019. Testing early warning metrics for drought-induced tree physiological stress and mortality. Glob. Change Biol. 25 (7), 2459–2469. https://doi.org/10.1111/gcb.14655.

Archambault, S., Bergeron, Y., 1992. An 802-year tree-ring chronology from the Quebec boreal forest. Can. J. For. Res. 22 (5), 674–682. https://doi.org/10.1139/x92-090.

Asner, G.P., 1998. Biophysical and biochemical sources of variability in canopy reflectance. Remote Sens. Environ. 64 (3), 234–253. https://doi.org/10.1016/S0034-4257(98)00014-5.

Babst, F., Esper, J., Parlow, E., 2010. Landsat TM/ETM+ and tree-ring based assessment of spatiotemporal patterns of the autumnal moth (Epirrita autumnata) in northernmost Fennoscandia. Remote Sens. Environ. 114 (3), 637–646. https://doi.org/10.1016/j.rse.2009.11.005.

Babst, F., Bouriaud, O., Alexander, R., Trouet, V., Frank, D., 2014. Toward consistent measurements of carbon accumulation: a multi-site assessment of biomass and basal area increment across Europe. Dendrochronologia 32 (2), 153–161. https://doi.org/10.1016/j.dendro.2014.01.002.

Babst, F., Bodesheim, P., Charney, N., Friend, A.D., Girardin, M.P., Klesse, S., Moore, D.J. P., Seftigen, K., Björklund, J., Bouriaud, O., Dawson, A., DeRose, R.J., Dietze, M.C., Eckes, A.H., Enquist, B., Frank, D.C., Mahecha, M.D., Poulter, B., Record, S., Evans, M.E.K., 2018. When tree rings go global: challenges and opportunities for retro- and prospective insight. Quat. Sci. Rev. 197, 1–20. https://doi.org/10.1016/j.quascirev.2018.07.009.

Banskota, A., Kayastha, N., Falkowski, M.J., Wulder, M.A., Froese, R.E., White, J.C., 2014. Forest monitoring using landsat time series data: a review. Can. J. Remote Sens. 40 (5), 362–384. https://doi.org/10.1080/07038992.2014.987376.

Beck, P.S.A., Goetz, S.J., 2011. Satellite observations of high northern latitude vegetation productivity changes between 1982 and 2008: ecological variability and regional differences. Environ. Res. Lett. 6 (4), 045501 https://doi.org/10.1088/1748-9326/6/4/045501.

Bell, D.M., Cohen, W.B., Reilly, M., Yang, Z., 2018. Visual interpretation and time series modeling of Landsat imagery highlight drought's role in forest canopy declines. Ecosphere 9 (6), e02195. https://doi.org/10.1002/ecs2.2195.

Berner, L.T., Goetz, S.J., 2022. Satellite observations document trends consistent with a boreal forest biome shift. Glob. Change Biol. 28 (10), 3275–3292. https://doi.org/10.1111/gcb.16121.

Beven, K.J., Kirkby, M.J., 1979. A physically based, variable contributing area model of basin hydrology/Un modèle à base physique de zone d'appel variable de l'hydrologie du bassin versant. Hydrol. Sci. J. 24 (1), 43–69.

Bilyk, A., Pulkki, R., Shahi, C., Larocque, G.R., 2021. Development of the Ontario forest resources Inventory: a historical review. Can. J. For. Res. 51 (2), 198–209. https://doi.org/10.1139/cjfr-2020-0234.

Biondi, F., 1999. Comparing tree-ring chronologies and repeated timber inventories as forest monitoring tools. Ecol. Appl. 9 (1), 216–227. https://doi.org/10.1890/1051-0761(1999)009[0216:CTRCAR]2.0.CO;2.

Biondi, F., Qeadan, F., 2008. A theory-driven approach to tree-ring standardization: defining the biological trend from expected basal area increment. Tree-Ring Res. 64 (2), 81–96. https://doi.org/10.3959/2008-6.1.

Blais, J.R., 1957. Some relationships of the spruce budworm, choristoneura fumiferana (clem.) to black spruce, Picea mariana (moench) voss. For. Chron. 33 (4), 364–372. https://doi.org/10.5558/tfc33364-4.

Boisvenue, C., White, J.C., 2019. Information needs of next-generation forest carbon models: opportunities for remote sensing science. Article 4. Remote Sens. 11 (4) https://doi.org/10.3390/rs11040463.

Bonney, M.T., He, Y., 2021. Temporal connections between long-term Landsat time-series and tree-rings in an urban–rural temperate forest. Int. J. Appl. Earth Obs. Geoinf. 103, 102523 https://doi.org/10.1016/j.jag.2021.102523.

Bouchard, M., Auger, I., 2014. Influence of environmental factors and spatio-temporal covariates during the initial development of a spruce budworm outbreak. Landsc. Ecol. 29 (1), 111–126. https://doi.org/10.1007/s10980-013-9966-x.

Bouchard, M., Régnière, J., Therrien, P., 2018. Bottom-up factors contribute to large-scale synchrony in spruce budworm populations. Can. J. For. Res. 48 (3), 277–284. https://doi.org/10.1139/cjfr-2017-0051.

Boulanger, Y., Arseneault, D., 2004. Spruce budworm outbreaks in eastern Quebec over the last 450 years. Can. J. For. Res. 34 (5), 1035–1043. https://doi.org/10.1139/x03-269.

Brandt, J.P., Flannigan, M.D., Maynard, D.G., Thompson, I.D., Volney, W.J.A., 2013. An introduction to Canada's boreal zone: ecosystem processes, health, sustainability, and environmental issues. Environ. Rev. 21 (4), 207–226. https://doi.org/10.1139/er-2013-0040.

Brecka, A.F.J., Shahi, C., Chen, H.Y.H., 2018. Climate change impacts on boreal forest timber supply. For. Policy Econ. 92, 11–21. https://doi.org/10.1016/j.forpol.2018.03.010.

Brienen, R.J.W., Zuidema, P.A., Martínez-Ramos, M., 2010. Attaining the canopy in dry and moist tropical forests: strong differences in tree growth trajectories reflect variation in growing conditions. Oecologia 163 (2), 485–496. https://doi.org/10.1007/s00442-009-1540-5.

Bufton, J.L., Garvin, J.B., Cavanaugh, J.F., Ramos-Izquierdo, L.A., Clem, T.D., Krabill, W. B., 1991. Airborne lidar for profiling of surface topography. Opt. Eng. 30 (1), 72–78. https://doi.org/10.1117/12.55770.

Canelles, Q., Aquilué, N., James, P.M.A., Lawler, J., Brotons, L., 2021. Global review on interactions between insect pests and other forest disturbances. Landsc. Ecol. 36 (4), 945–972. https://doi.org/10.1007/s10980-021-01209-7.

Chagnon, C., Wotherspoon, A.R., Achim, A., 2022. Deciphering the black spruce response to climate variation across eastern Canada using a meta-analysis approach. For. Ecol. Manag. 520, 120375 https://doi.org/10.1016/j.foreco.2022.120375.

Chen, W., Chen, J.M., Price, D.T., Cihlar, J., 2002. Effects of stand age on net primary productivity of boreal black spruce forests in Ontario, Canada. Can. J. For. Res. 32 (5), 833–842. https://doi.org/10.1139/x01-165.

Conrad, O., Bechtel, B., Bock, M., Dietrich, H., Fischer, E., Gerlitz, L., Wehberg, J., Wichmann, V., Böhner, J., 2015. System for automated geoscientific analyses (SAGA) v. 2.1.4. Geosci. Model Dev. 8 (7), 1991–2007. https://doi.org/10.5194/gmd-8-1991-2015.

Coops, N.C., 2015. Characterizing forest growth and productivity using remotely sensed data. Curr. For. Rep. 1 (3), 195–205. https://doi.org/10.1007/s40725-015-0020-x.

Coops, N.C., Shang, C., Wulder, M.A., White, J.C., Hermosilla, T., 2020. Change in forest condition: characterizing non-stand replacing disturbances using time series satellite imagery. For. Ecol. Manag. 474, 118370 https://doi.org/10.1016/j.foreco.2020.118370.

Coops, N.C., Tompalski, P., Goodbody, T.R.H., Achim, A., Mulverhill, C., 2023. Framework for near real-time forest inventory using multi source remote sensing data. For.: Int. J. For. Res. 96 (1), 1–19. https://doi.org/10.1093/forestry/cpac015.

Crist, E.P., 1985. A TM Tasseled Cap equivalent transformation for reflectance factor data. Remote Sens. Environ. 17 (3), 301–306. https://doi.org/10.1016/0034-4257(85)90102-6.

Czerwinski, C.J., King, D.J., Mitchell, S.W., 2014. Mapping forest growth and decline in a temperate mixed forest using temporal trend analysis of Landsat imagery, 1987-2010. Remote Sens. Environ. 141, 188–200. https://doi.org/10.1016/j.rse.2013.11.006.

D'Orangeville, L., Houle, D., Duchesne, L., Phillips, R.P., Bergeron, Y., Kneeshaw, D., 2018. Beneficial effects of climate warming on boreal tree growth may be transitory. Nat. Commun. 9 (1), 3213. https://doi.org/10.1038/s41467-018-05705-4.

De Grandpré, L., Kneeshaw, D.D., Perigon, S., Boucher, D., Marchand, M., Pureswaran, D., Girardin, M.P., 2019. Adverse climatic periods precede and amplify defoliator-induced tree mortality in eastern boreal North America. J. Ecol. 107 (1), 452–467. https://doi.org/10.1111/1365-2745.13012.

Decuyper, M., Chávez, R.O., Čufar, K., Estay, S.A., Clevers, J.G.P.W., Prislan, P., Gričar, J., Črepinšek, Z., Merela, M., de Luis, M., Notivoli, R.S., del Castillo, E.M., Rozendaal, D.M.A., Bongers, F., Herold, M., Sass-Klaassen, U., 2020. Spatio-temporal assessment of beech growth in relation to climate extremes in Slovenia – An integrated approach using remote sensing and tree-ring data. Agric. For. Meteorol. 287, 107925 https://doi.org/10.1016/j.agrformet.2020.107925.

DeSoto, L., Cailleret, M., Sterck, F., Jansen, S., Kramer, K., Robert, E.M.R., Aakala, T., Amoroso, M.M., Bigler, C., Camarero, J.J., Čufar, K., Gea-Izquierdo, G., Gillner, S., Haavik, L.J., Hereş, A.-M., Kane, J.M., Kharuk, V.I., Kitzberger, T., Klein, T., Martínez-Vilalta, J., 2020. Low growth resilience to drought is related to future mortality risk in trees. Article 1. Nat. Commun. 11 (1) https://doi.org/10.1038/s41467-020-14300-5.

Dottavio, C.L., Williams, D.L., 1983. Satellite technology: an improved means for monitoring forest insect defoliation. J. For. 81 (1), 30–34. https://doi.org/10.1093/jof/81.1.30.

Fassnacht, F.E., Hartig, F., Latifi, H., Berger, C., Hernández, J., Corvalán, P., Koch, B., 2014. Importance of sample size, data type and prediction method for remote sensing-based estimations of aboveground forest biomass. Remote Sens. Environ. 154, 102–114.

Fiore, N.M., Goulden, M.L., Czimczik, C.I., Pedron, S.A., Tayo, M.A., 2020. Do recent NDVI trends demonstrate boreal forest decline in Alaska? Environ. Res. Lett. 15 (9), 095007 https://doi.org/10.1088/1748-9326/ab9c4c.

Foster, A.C., Wang, J.A., Frost, G.V., Davidson, S.J., Hoy, E., Turner, K.W., Goetz, S., 2022. Disturbances in North American boreal forest and Arctic tundra: impacts, interactions, and responses. Environ. Res. Lett. 17 (11), 113001.
Franklin, S.E., Lavigne, M.B., Moskal, L.M., Wulder, M.A., McCaffrey, T.M., 2001. Interpretation of forest harvest conditions in new brunswick using landsat tm enhanced wetness difference imagery (EWDI). Can. J. Remote Sens. 27 (2), 118–128. https://doi.org/10.1080/07038992.2001.10854926.
Gauthier, S., Bernier, P., Kuuluvainen, T., Shvidenko, A.Z., Schepaschenko, D.G., 2015. Boreal forest health and global change. Science 349 (6250), 819–822. https://doi.org/10.1126/science.aaa9092.
Gazol, A., Camarero, J.J., Gutiérrez, E., Popa, I., Andreu-Hayles, L., Motta, R., Carrer, M., 2015. Distinct effects of climate warming on populations of silver fir (Abies alba) across Europe. J. Biogeogr. 42 (6), 1150–1162.
Gazol, A., Camarero, J.J., Vicente-Serrano, S.M., Sánchez-Salguero, R., Gutiérrez, E., de Luis, M., Sangüesa-Barreda, G., Novak, K., Rozas, V., Tíscar, P.A., Linares, J.C., Martín-Hernández, N., Martínez del Castillo, E., Ribas, M., García-González, I., Silla, F., Camisón, A., Génova, M., Olano, J.M., Galván, J.D., 2018. Forest resilience to drought varies across biomes. Glob. Change Biol. 24 (5), 2143–2158. https://doi.org/10.1111/gcb.14082.
Gillis, M.D., Omule, A.Y., Brierley, T., 2005. Monitoring Canada's forests: the national forest inventory. For. Chron. 81 (2), 214–221. https://doi.org/10.5558/tfc81214-2.
Girardin, M.P., Raulier, F., Bernier, P.Y., Tardif, J.C., 2008. Response of tree growth to a changing climate in boreal central Canada: a comparison of empirical, process-based, and hybrid modelling approaches. Ecol. Model. 213 (2), 209–228. https://doi.org/10.1016/j.ecolmodel.2007.12.010.
Girardin, M.P., Bouriaud, O., Hogg, E.H., Kurz, W., Zimmermann, N.E., Metsaranta, J.M., de Jong, R., Frank, D.C., Esper, J., Büntgen, U., Guo, X.J., Bhatti, J., 2016. No growth stimulation of Canada's boreal forest under half-century of combined warming and CO 2 fertilization. Proc. Natl. Acad. Sci. 113 (52), E8406–E8414. https://doi.org/10.1073/pnas.1610156113.
Girardin, M.P., Guo, X.J., Metsaranta, J., Gervais, D., Campbell, E., Arsenault, A., Hogg, E.H., 2021. A national tree-ring data repository for Canadian forests (CFS-TRenD): structure, synthesis, and applications. Environ. Rev. 29 (2), 225–241.
Grissino-Mayer, H.D., Fritts, H.C., 1997. The international tree-ring data bank: an enhanced global database serving the global scientific community—Henri D. Grissino-Mayer, Harold C. Fritts 1997 https://journals.sagepub.com/doi/abs/10.1177/095968369700700212.
Guibal, F., Guiot, J., 2021. Dendrochronology. In: Ramstein, G., Landais, A., Bouttes, N., Sepulchre, P., Govin, A. (Eds.), Paleoclimatology. Springer International Publishing, pp. 117–122. https://doi.org/10.1007/978-3-030-24982-3_8.
Harper, K., Bergeron, Y., Gauthier, S., Drapeau, P., 2002. Post-fire development of canopy structure and composition in black spruce forests of Abitibi, Québec: a landscape scale study. Silva Fenn. 36 (1) https://doi.org/10.14214/sf.561.
Harper, K., Bergeron, Y., Drapeau, P., Gauthier, S., De Grandpré, L., 2005. Structural development following fire in black spruce boreal forest. For. Ecol. Manag. 206 (1), 293–306. https://doi.org/10.1016/j.foreco.2004.11.008.
Healey, S.P., Yang, Z., Cohen, W.B., Pierce, D.J., 2006. Application of two regression-based methods to estimate the effects of partial harvest on forest structure using Landsat data. Remote Sens. Environ. 101 (1), 115–126. https://doi.org/10.1016/j.rse.2005.12.006.
Hennigar, C.R., MacLean, D.A., Quiring, D.T., Kershaw Jr, J.A., 2008. Differences in spruce budworm defoliation among balsam fir and white, red, and black spruce. For. Sci. 54 (2), 158–166. https://doi.org/10.1093/forestscience/54.2.158.
Hermosilla, T., Wulder, M.A., White, J.C., Coops, N.C., Hobart, G.W., 2015b. Regional detection, characterization, and attribution of annual forest change from 1984 to 2012 using Landsat-derived time-series metrics. Remote Sens. Environ. 170, 121–132. https://doi.org/10.1016/j.rse.2015.09.004.
Hermosilla, T., Wulder, M.A., White, J.C., Coops, N.C., Hobart, G.W., 2015a. An integrated Landsat time series protocol for change detection and generation of annual gap-free surface reflectance composites. Remote Sens. Environ. 158, 220–234. https://doi.org/10.1016/j.rse.2014.11.005.
Hijmans, R.J., Bivand, R., Forner, K., Ooms, J., Pebesma, E., Sumner, M.D., 2022. Package 'terra'. Maint.: Vienna, Austria.
Hodkinson, I.D., 2005. Terrestrial insects along elevation gradients: species and community responses to altitude. Biol. Rev. 80 (3), 489–513. https://doi.org/10.1017/S1464793105006767.
Holmes, R.L., 1983. Computer-assisted quality control in tree-ring dating and mearurement. Tree-Ring Bull. 43, 69–78.
Isaacs, R.E., Stueve, K.M., Lafon, C.W., Taylor, A.H., 2014. Ice storms generate spatially heterogeneous damage patterns at the watershed scale in forested landscapes. Ecosphere 5 (11), art141. https://doi.org/10.1890/ES14-00234.1.
Itter, M.S., D'Orangeville, L., Dawson, A., Kneeshaw, D., Duchesne, L., Finley, A.O., 2019. Boreal tree growth exhibits decadal-scale ecological memory to drought and insect defoliation, but no negative response to their interaction. J. Ecol. 107 (3), 1288–1301. https://doi.org/10.1111/1365-2745.13087.
Jactel, H., Petit, J., Desprez-Loustau, M.-L., Delzon, S., Piou, D., Battisti, A., Koricheva, J., 2012. Drought effects on damage by forest insects and pathogens: a meta-analysis. Glob. Change Biol. 18 (1), 267–276. https://doi.org/10.1111/j.1365-2486.2011.02512.x.
James, P.M.A., Robert, L.-E., Wotton, B.M., Martell, D.L., Fleming, R.A., 2017. Lagged cumulative spruce budworm defoliation affects the risk of fire ignition in Ontario, Canada. Ecol. Appl. 27 (2), 532–544. https://doi.org/10.1002/eap.1463.
Kannenberg, S.A., Schwalm, C.R., Anderegg, W.R.L., 2020. Ghosts of the past: how drought legacy effects shape forest functioning and carbon cycling. Ecol. Lett. 23 (5), 891–901. https://doi.org/10.1111/ele.13485.
Kéfi, S., Dakos, V., Scheffer, M., Van Nes, E.H., Rietkerk, M., 2013. Early warning signals also precede non-catastrophic transitions. Oikos 122 (5), 641–648. https://doi.org/10.1111/j.1600-0706.2012.20838.x.
Kennedy, R.E., Yang, Z., Cohen, W.B., 2010. Detecting trends in forest disturbance and recovery using yearly Landsat time series: 1. LandTrendr — Temporal segmentation algorithms. Remote Sens. Environ. 114 (12), 2897–2910. https://doi.org/10.1016/j.rse.2010.07.008.
Key, C.H., & Benson, N.C. (2006). Landscape assessment (LA). In: Lutes, Duncan C.; Keane, Robert E.; Caratti, John F.; Key, Carl H.; Benson, Nathan C.; Sutherland, Steve; Gangi, Larry J. 2006. FIREMON: Fire Effects Monitoring and Inventory System. Gen. Tech. Rep. RMRS-GTR-164-CD. Fort Collins, CO: US Department of Agriculture, Forest Service, Rocky Mountain Research Station. p. LA-1-55, 164.
Kim, J.H., 2009. Estimating classification error rate: repeated cross-validation, repeated hold-out and bootstrap. Comput. Stat. data Anal. 53 (11), 3735–3745.
Klesse, S., Etzold, S., Frank, D., 2016. Integrating tree-ring and inventory-based measurements of aboveground biomass growth: research opportunities and carbon cycle consequences from a large snow breakage event in the Swiss Alps. Eur. J. For. Res. 135 (2), 297–311. https://doi.org/10.1007/s10342-015-0936-5.
Lacey, M., Dech, J., 2012. Comparison of black spruce (Picea mariana) radial growth reduction in different soil moisture regimes during a spruce budworm (Choristoneura fumiferana) outbreak. Can. J. For. Res. 42, 1410–1419. https://doi.org/10.1139/x2012-080.
LeBlanc, D.C., 1990. Red spruce decline on Whiteface Mountain, New York. I. Relationships with elevation, tree age, and competition. Can. J. For. Res. 20 (9), 1408–1414. https://doi.org/10.1139/x90-186.
Lieffers, V., Messier, C., Burton, P., Ruel, J.-C., Grover, B., 2003. Nat.-Based Silvic. Sustain. a Var. Boreal For. Values 481–530.
Liu, X., 2008. Airborne LiDAR for DEM generation: some critical issues. Progress. Phys. Geogr.: Earth Environ. 32 (1), 31–49. https://doi.org/10.1177/0309133308089496.
Liu, Y., Kumar, M., Katul, G.G., Porporato, A., 2019. Reduced resilience as an early warning signal of forest mortality. Nat. Clim. Change 9 (11), 880–885. https://doi.org/10.1038/s41558-019-0583-9.
Lloyd, A.H., Duffy, P.A., Mann, D.H., 2013. Nonlinear responses of white spruce growth to climate variability in interior Alaska. Can. J. For. Res. 43 (4), 331–343. https://doi.org/10.1139/cjfr-2012-0372.
Lopatin, E., Kolström, T., Spiecker, H., 2006. Determ. For. Growth Trends Komi Repub. (Northwest. Russ.): Comb. tree-ring Anal. Remote Sens. data 11, 14.
Magnussen, S., Boudewyn, P., Alfaro, R., 2004. Spatial prediction of the onset of spruce budworm defoliation. For. Chron. 80 (4), 485–494. https://doi.org/10.5558/tfc80485-4.
Mahony, C.R., Wang, T., Hamann, A., Cannon, A.J., 2022. A global climate model ensemble for downscaled monthly climate normals over North America. Int. J. Climatol. 42 (11), 5871–5891.
Mallet, C., Bretar, F., 2009. Full-waveform topographic lidar: state-of-the-art. ISPRS J. Photogramm. Remote Sens. 64 (1), 1–16. https://doi.org/10.1016/j.isprsjprs.2008.09.007.
Mamet, S.D., Chun, K.P., Metsaranta, J.M., Barr, A.G., Johnstone, J.F., 2015. Tree rings provide early warning signals of jack pine mortality across a moisture gradient in the southern boreal forest. Environ. Res. Lett. 10 (8), 084021 https://doi.org/10.1088/1748-9326/10/8/084021.
Marchand, W., Girardin, M.P., Hartmann, H., Gauthier, S., Bergeron, Y., 2019. Taxonomy, together with ontogeny and growing conditions, drives needleleaf species' sensitivity to climate in boreal North America. Glob. Change Biol. 25 (8), 2793–2809. https://doi.org/10.1111/gcb.14665.
Matasci, G., Hermosilla, T., Wulder, M.A., White, J.C., Coops, N.C., Hobart, G.W., Zald, H.S.J., 2018. Large-area mapping of Canadian boreal forest cover, height, biomass and other structural attributes using Landsat composites and lidar plots. Remote Sens. Environ. 209, 90–106. https://doi.org/10.1016/j.rse.2017.12.020.
Mazerolle, M.J. (2020). AICcmodavg: Model selection and multimodel inference based on (Q)AIC(c). R package version 2.3-1. https://cran.r-project.org/package=AICcmodavg.
McDowell, N.G., Allen, C.D., Anderson-Teixeira, K., Aukema, B.H., Bond-Lamberty, B., Chini, L., Clark, J.S., Dietze, M., Grossiord, C., Hanbury-Brown, A., others, 2020. Pervasive shifts in forest dynamics in a changing world. Science 368 (6494), eaaz9463.
McKenney, D.W., Pedlar, J.H., Papadopol, P., Hutchinson, M.F., 2006. The development of 1901–2000 historical monthly climate models for Canada and the United States. Agric. For. Meteorol. 138 (1), 69–81. https://doi.org/10.1016/j.agrformet.2006.03.012.
MFFP. (2018). Ressources et industries forestières du Québec: Portrait statistique 2018. Ministère des Forêts, de la Faune et des Parcs, Direction de la modernisation de l'industrie des produits forestiers.
MNRF. (2021). Forest resources of Ontario 2021. https://www.ontario.ca/document/forest-resources-ontario-2021.
MNRF. (2023a). Forest Abiotic Damage Event. Ministry of Natural Resources and Forests. https://geohub.lio.gov.on.ca/datasets/lio::forest-abiotic-damage-event/about.
MNRF. (2023b). Forest Insect Damage Event. Ministry of Natural Resources and Forests. https://geohub.lio.gov.on.ca/documents/forest-insect-damage-event/about.
Moreau, G., Achim, A., Pothier, D., 2020. An accumulation of climatic stress events has led to years of reduced growth for sugar maple in southern Quebec, Canada. Ecosphere 11 (7), e03183.
Moreau, G., Chagnon, C., Achim, A., Caspersen, J., D'Orangeville, L., Sánchez-Pinillos, M., Thiffault, N., 2022. Opportunities and limitations of thinning to increase resistance and resilience of trees and forests to global change. Forestry 95 (5), 595–615.

Morin-Bernard, A., Achim, A., Coops, N.C., 2023a. Attributing a causal agent and assessing the severity of non-stand replacing disturbances in a northern hardwood forest using landsat-derived vegetation indices. Can. J. Remote Sens. https://doi.org/10.1080/07038992.2023.2196356.

Morin-Bernard, A., Coops, N.C., White, J.C., Achim, A., 2023b. Predicting net growth rates in boreal forests using Landsat time series and permanent sample plot data. For.: Int. J. For. Res. https://doi.org/10.1093/forestry/cpad055.

MRNF. (2022). Cartographie du cinquième inventaire écoforestier du Québec méridional—Méthodes et données associées (p. 129). Ministère des Ressources naturelles et des Forêts, Secteur des forêts, Direction des inventaires forestiers.

MRNF. (2023). Données sur les perturbations naturelles – insecte: Tordeuse des bourgeons de l'épinette. Ministère des Ressources naturelles et des Forêts, Secteur des forêts. https://www.donneesquebec.ca/recherche/fr/dataset/donnees-sur-les-perturbations-naturelles-insecte-tordeuse-des-bourgeons-de-lepinette.

Mulverhill, C., Coops, N.C., Achim, A., 2023. Continuous monitoring and sub-annual change detection in high-latitude forests using Harmonized Landsat Sentinel-2 data. ISPRS J. Photogramm. Remote Sens. 197, 309–319. https://doi.org/10.1016/j.isprsjprs.2023.02.002.

Nabuurs, G.J., Andrasko, K., Benitez-Ponce, P., Boer, R., Dutschke, M., Elsiddig, E., Ford-Robertson, J., Matsumoto, M., Oyhantcabal, W., Achard, F., Anaya, C., Brinkman, S., Higuchi, N., Hoogwijk, M., Lecocq, F., Rose, S., Schlamadinger, B., Filho, B.S.S., Sohngen, B., … Calvo, E. (2007). Chapter 9—Forestry. IPCC, Cambridge University Press, Cambridge, UK and New York, NY, USA., 44.

Næsset, E., 2002. Predicting forest stand characteristics with airborne laser scanning using a practical two-stage procedure and field data. Remote Sens. Environ. 80, 88–99. https://doi.org/10.1016/S0034-4257(01)00290-5.

Nehrbass-Ahles, C., Babst, F., Klesse, S., Nötzli, M., Bouriaud, O., Neukom, R., Dobbertin, M., Frank, D., 2014. The influence of sampling design on tree-ring-based quantification of forest growth. Glob. Change Biol. 20 (9), 2867–2885. https://doi.org/10.1111/gcb.12599.

Ohlson, M., Dahlberg, B., Økland, T., Brown, K.J., Halvorsen, R., 2009. The charcoal carbon pool in boreal forest soils. Article 10. Nat. Geosci. 2 (10) https://doi.org/10.1038/ngeo617.

Oliver, C.D., Larson, B.C., 1996. Forest stand dynamics. Wiley, New York.

Olthof, I., King, D.J., Lautenschlager, R.A., 2004. Mapping deciduous forest ice storm damage using Landsat and environmental data. Remote Sens. Environ. 89 (4), 484–496. https://doi.org/10.1016/j.rse.2003.11.010.

Pan, Y., Birdsey, R.A., Fang, J., Houghton, R., Kauppi, P.E., Kurz, W.A., Phillips, O.L., Shvidenko, A., Lewis, S.L., Canadell, J.G., Ciais, P., Jackson, R.B., Pacala, S.W., McGuire, A.D., Piao, S., Rautiainen, A., Sitch, S., Hayes, D., 2011. A large and persistent carbon sink in the World's Forests. Science 333 (6045), 988–993. https://doi.org/10.1126/science.1201609.

Payette, S., Delwaide, A., 2003. Shift of conifer boreal forest to lichen–heath parkland caused by successive stand disturbances. Ecosystems 6 (6), 540–550. https://doi.org/10.1007/PL00021507.

Peng, C., Ma, Z., Lei, X., Zhu, Q., Chen, H., Wang, W., Liu, S., Li, W., Fang, X., Zhou, X., 2011. A drought-induced pervasive increase in tree mortality across Canada's boreal forests. Nat. Clim. Change 1 (9), 467–471. https://doi.org/10.1038/nclimate1293.

Peñuelas, J., Hunt, J.M., Ogaya, R., Jump, A.S., 2008. Twentieth century changes of tree-ring δ13C at the southern range-edge of Fagus sylvatica: increasing water-use efficiency does not avoid the growth decline induced by warming at low altitudes. Glob. Change Biol. 14 (5), 1076–1088. https://doi.org/10.1111/j.1365-2486.2008.01563.x.

Perron, J.-Y., 1985. Tarif de cubage général: Volume marchand brut. [Serv.&[Service32; [Serv.

Primicia, I., Camarero, J.J., Janda, P., Čada, V., Morrissey, R.C., Trotsiuk, V., Svoboda, M., 2015. Age, competition, disturbance and elevation effects on tree and stand growth response of primary Picea abies forest to climate. For. Ecol. Manag. 354, 77–86.

Queinnec, M., Coops, N.C., White, J.C., McCartney, G., Sinclair, I., 2022. Developing a forest inventory approach using airborne single photon lidar data: from ground plot selection to forest attribute prediction. For.: Int. J. For. Res. 95 (3), 347–362. https://doi.org/10.1093/forestry/cpab051.

Ranganathan, P., Pramesh, C.S., Aggarwal, R., 2017. Common pitfalls in statistical analysis: logistic regression. Perspect. Clin. Res. 8 (3), 148–151. https://doi.org/10.4103/picr.PICR_87_17.

Régnière, J., St-Amant, R., Duval, P., 2012. Predicting insect distributions under climate change from physiological responses: spruce budworm as an example. Biol. Invasions 14 (8), 1571–1586. https://doi.org/10.1007/s10530-010-9918-1.

Régnière, J., Saint-Amant, R., Béchard, A., Moutaoufik, A., 2017. BioSIM 11–Manuel d'utilisation. Que., QC, Can.: Nat. Resour. Can., Can. For. Serv., Laurent. For. Cent.

Riopel, M., Munger, D., Leboeuf, A., Bergeron, C., & Lefrançois, R. (2022). Carte dendrométrique LiDAR – Méthode et utilisation—2e édition (p. 32). Ministère des Ressources naturelles et des Forêts, Secteur des forêts, Direction des inventaires forestiers.

Rodman, K.C., Andrus, R.A., Veblen, T.T., Hart, S.J., 2021. Disturbance detection in landsat time series is influenced by tree mortality agent and severity, not by prior disturbance. Remote Sens. Environ. 254, 112244 https://doi.org/10.1016/j.rse.2020.112244.

Rodriguez, J.D., Perez, A., Lozano, J.A., 2009. Sensitivity analysis of k-fold cross validation in prediction error estimation. IEEE Trans. Pattern Anal. Mach. Intell. 32 (3), 569–575.

Šamonil, P., Kotík, L., Vašíčková, I., 2015. Uncertainty in detecting the disturbance history of forest ecosystems using dendrochronology. Dendrochronologia 35, 51–61.

Sánchez-Pinillos, M., Leduc, A., Ameztegui, A., Kneeshaw, D., Lloret, F., Coll, L., 2019. Resistance, resilience or change: post-disturbance dynamics of boreal forests after insect outbreaks. Ecosystems 22 (8), 1886–1901. https://doi.org/10.1007/s10021-019-00378-6.

Sánchez-Pinillos, M., D'Orangeville, L., Boulanger, Y., Comeau, P., Wang, J., Taylor, A. R., Kneeshaw, D., 2022. Sequential droughts: a silent trigger of boreal forest mortality. Glob. Change Biol. 28 (2), 542–556. https://doi.org/10.1111/gcb.15913.

Saucier, J.-P., Gosselin, J., Morneau, C., Grondin, P., 2010. Utilisation de la classification de la végétation dans l'aménagement forestier au Québec. Rev. Forère Française 62 (3–4), 428–438.

Seidl, R., Thom, D., Kautz, M., Martin-Benito, D., Peltoniemi, M., Vacchiano, G., Wild, J., Ascoli, D., Petr, M., Honkaniemi, J., Lexer, M.J., Trotsiuk, V., Mairota, P., Svoboda, M., Fabrika, M., Nagel, T.A., Reyer, C.P.O., 2017. Forest disturbances under climate change. Article 6. Nat. Clim. Change 7 (6) https://doi.org/10.1038/nclimate3303.

Sen, P.K., 1968. Estimates of the regression coefficient based on Kendall's tau. J. Am. Stat. Assoc. 63 (324), 1379–1389.

Senf, C., Pflugmacher, D., Wulder, M.A., Hostert, P., 2015. Characterizing spectral–temporal patterns of defoliator and bark beetle disturbances using Landsat time series. Remote Sens. Environ. 170, 166–177. https://doi.org/10.1016/j.rse.2015.09.019.

Senf, C., Seidl, R., Hostert, P., 2017. Remote sensing of forest insect disturbances: current state and future directions. Int. J. Appl. Earth Obs. Geoinf. 60, 49–60. https://doi.org/10.1016/j.jag.2017.04.004.

Shapiro, S.S., Wilk, M.B., 1965. An analysis of variance test for normality (complete samples). Biometrika 52 (3/4), 591–611.

Smyth, C.E., Stinson, G., Neilson, E., Lemprière, T.C., Hafer, M., Rampley, G.J., Kurz, W. A., 2014. Quantifying the biophysical climate change mitigation potential of Canada's forest sector. Biogeosciences 11 (13), 3515–3529. https://doi.org/10.5194/bg-11-3515-2014.

Sulla-Menashe, D., Woodcock, C.E., Friedl, M.A., 2018. Canadian boreal forest greening and browning trends: an analysis of biogeographic patterns and the relative roles of disturbance versus climate drivers. Environ. Res. Lett. 13 (1), 014007 https://doi.org/10.1088/1748-9326/aa9b88.

Sullivan, P.F., Pattison, R.R., Brownlee, A.H., Cahoon, S.M.P., Hollingsworth, T.N., 2016. Effect of tree-ring detrending method on apparent growth trends of black and white spruce in interior Alaska. Environ. Res. Lett. 11 (11), 114007 https://doi.org/10.1088/1748-9326/11/11/114007.

Theil, H., 1950. A rank-invariant method of linear and polynomial regression analysis. Indag. Math. 12 (85), 173.

Tjur, T., 2009. Coefficients of determination in logistic regression models—A new proposal: the coefficient of discrimination. Am. Stat. 63 (4), 366–372.

Torresan, C., Benito Garzón, M., O'Grady, M., Robson, T.M., Picchi, G., Panzacchi, P., Tomelleri, E., Smith, M., Marshall, J., Wingate, L., Tognetti, R., Rustad, L.E., Kneeshaw, D., 2021. A new generation of sensors and monitoring tools to support climate-smart forestry practices. Can. J. For. Res. 51 (12), 1751–1765. https://doi.org/10.1139/cjfr-2020-0295.

Trotsiuk, V., Pederson, N., Druckenbrod, D.L., Orwig, D.A., Bishop, D.A., Barker-Plotkin, A., Fraver, S., Martin-Benito, D., 2018. Testing the efficacy of tree-ring methods for detecting past disturbances. For. Ecol. Manag. 425, 59–67. https://doi.org/10.1016/j.foreco.2018.05.045.

Tucker, C.J., 1979. Red and photographic infrared linear combinations for monitoring vegetation. Remote Sens. Environ. 8, 127.

Urquizo, N., Bastedo, J., Brydges, T., & Shear, H. (2000). Ecological assessment of the boreal shield ecozone (p. 90 p.). Environment Canada. https://publications.gc.ca/collections/collection_2014/ec/En40-600-2000-eng.pdf.

Verbyla, A.P., 1993. Modelling variance heterogeneity: residual maximum likelihood and diagnostics. J. R. Stat. Soc.: Ser. B Methodol. 55 (2), 493–508.

Vicente-Serrano, S.M., Beguería, S., López-Moreno, J.I., 2010. A multiscalar drought index sensitive to global warming: the standardized precipitation evapotranspiration index. J. Clim. 23 (7), 1696–1718. https://doi.org/10.1175/2009JCLI2909.1.

Vicente-Serrano, S.M., Camarero, J.J., Olano, J.M., Martín-Hernández, N., Peña-Gallardo, M., Tomás-Burguera, M., Gazol, A., Azorin-Molina, C., Bhuyan, U., El Kenawy, A., 2016. Diverse relationships between forest growth and the normalized difference vegetation index at a global scale. Remote Sens. Environ. 187, 14–29. https://doi.org/10.1016/j.rse.2016.10.001.

Vogelmann, J.E., Gallant, A.L., Shi, H., Zhu, Z., 2016. Perspectives on monitoring gradual change across the continuity of Landsat sensors using time-series data. Remote Sens. Environ. 185, 258–270. https://doi.org/10.1016/j.rse.2016.02.060.

Walker, X.J., Mack, M.C., Johnstone, J.F., 2015. Stable carbon isotope analysis reveals widespread drought stress in boreal black spruce forests. Glob. Change Biol. 21 (8), 3102–3113. https://doi.org/10.1111/gcb.12893.

Wang, J.A., Baccini, A., Farina, M., Randerson, J.T., Friedl, M.A., 2021. Disturbance suppresses the aboveground carbon sink in North American boreal forests. Article 5. Nat. Clim. Change 11 (5) https://doi.org/10.1038/s41558-021-01027-4.

Wester, M., Henson, B., Crins, W., Uhlig, P., Gray, P., others, 2018. The ecosystems of Ontario, Part 2: Ecodistricts. Sci. Res. Tech. Report.-Ont. Minist. Nat. Resour. For. TR-26.

White, J.C., Wulder, M.A., Varhola, A., Vastaranta, M., Coops, N.C., Cook, B.D., et al., 2013a. A best practices guide for generating forest inventory attributes from airborne laser scanning data using an area-based approach. Nat. Resour. Can. Can. For. Serv. Can. Wood Fibre Cent. Vic. Bc. Inf. Report. FI-X-010 https://cfs.nrcan.gc.ca/publications?id=34887.

White, J.C., Wulder, M.A., Hobart, G.W., Luther, J.E., Hermosilla, T., Griffiths, P., Coops, N.C., Hall, R.J., Hostert, P., Dyk, A., Guindon, L., 2014. Pixel-based image compositing for large-area dense time series applications and science. Can. J. Remote Sens. 40 (3), 192–212. https://doi.org/10.1080/07038992.2014.945827.

White, J.C., Wulder, M.A., Hermosilla, T., Coops, N.C., Hobart, G.W., 2017. A nationwide annual characterization of 25 years of forest disturbance and recovery for Canada using Landsat time series. Remote Sens. Environ. 194, 303–321.

Wolken, J.M., Mann, D.H., Grant, T.A., Lloyd, A.H., Rupp, T.S., Hollingsworth, T.N., 2016. Climate-growth relationships along a black spruce toposequence in interior Alaska. Arct. Antarct. Alp. Res. 48 (4), 637–652. https://doi.org/10.1657/AAAR0015-056.

Woodcock, C.E., Allen, R., Anderson, M., Belward, A., Bindschadler, R., Cohen, W., Gao, F., Goward, S.N., Helder, D., Helmer, E., others, 2008. Free access to landsat imagery. Sci. Vol. 320, 1011.

Woodcock, C.E., Loveland, T.R., Herold, M., Bauer, M.E., 2020. Transitioning from change detection to monitoring with remote sensing: a paradigm shift. Remote Sens. Environ. 238, 111558 https://doi.org/10.1016/j.rse.2019.111558.

Wotherspoon, A., Duchesne, L., Barrette, M., Houle, D., 2022b. Pre-commercial thinning could mitigate drought stress of black spruce stands. For. Ecol. Manag. 517, 120278 https://doi.org/10.1016/j.foreco.2022.120278.

Wotherspoon, A., Burnett, M., Bernard, A., Achim, A., Coops, N.C., 2022a. Clim. Scenar. Can. For. https://doi.org/10.13140/RG.2.2.18449.92009.

Wu, X., Liu, H., Li, X., Ciais, P., Babst, F., Guo, W., Zhang, C., Magliulo, V., Pavelka, M., Liu, S., Huang, Y., Wang, P., Shi, C., Ma, Y., 2018. Differentiating drought legacy effects on vegetation growth over the temperate Northern Hemisphere. Glob. Change Biol. 24 (1), 504–516. https://doi.org/10.1111/gcb.13920.

Wulder, M.A., Roy, D.P., Radeloff, V.C., Loveland, T.R., Anderson, M.C., Johnson, D.M., Healey, S., Zhu, Z., Scambos, T.A., Pahlevan, N., Hansen, M., Gorelick, N., Crawford, C.J., Masek, J.G., Hermosilla, T., White, J.C., Belward, A.S., Schaaf, C., Woodcock, C.E., Cook, B.D., 2022. Fifty years of landsat science and impacts. Remote Sens. Environ. 280, 113195 https://doi.org/10.1016/j.rse.2022.113195.

Zald, H.S.J., Wulder, M.A., White, J.C., Hilker, T., Hermosilla, T., Hobart, G.W., Coops, N.C., 2016. Integrating Landsat pixel composites and change metrics with lidar plots to predictively map forest structure and aboveground biomass in Saskatchewan, Canada. Remote Sens. Environ. 176, 188–201. https://doi.org/10.1016/j.rse.2016.01.015.

Zhao, S., Pederson, N., D'Orangeville, L., HilleRisLambers, J., Boose, E., Penone, C., Bauer, B., Jiang, Y., Manzanedo, R.D., 2019. The International Tree-Ring Data Bank (ITRDB) revisited: data availability and global ecological representativity. J. Biogeogr. 46 (2), 355–368.

Zhu, Z., Woodcock, C.E., 2014. Continuous change detection and classification of land cover using all available Landsat data. Remote Sens. Environ. 144, 152–171. https://doi.org/10.1016/j.rse.2014.01.011.

Zuur, A.F., Ieno, E.N., Elphick, C.S., 2010. A protocol for data exploration to avoid common statistical problems. Methods Ecol. Evol. 1 (1), 3–14.